AGU PUBLICATIONS

Radio Science

RESEARCH ARTICLE
10.1002/2017RS006340

Key Points:
- A new algorithm is proposed here for direction finding, for polarization estimation and for blind calibration for nonideal vector sensors
- This is achieved here by exploiting the electromagnetic vector sensor's quintessential array manifold
- This is achieved also by judiciously breaking down the originally high-dimensional problem into well chosen low-dimensional subproblems

Correspondence to:
K. T. Wong,
ktwong@ieee.org

Citation:
Song, Y., K. T. Wong, and F. Chen (2017), "Blind" calibration of vector sensors whose dipole/loop triads deviate from their nominal gains/phases/orientations/locations, *Radio Sci.*, *52*, 1170–1189, doi:10.1002/2017RS006340.

Received 19 APR 2017
Accepted 2 AUG 2017
Accepted article online 9 AUG 2017
Published online 19 SEP 2017

"Blind" calibration of vector sensors whose dipole/loop triads deviate from their nominal gains/phases/orientations/locations

Yang Song[1], Kainam Thomas Wong[2], and Fangjiong Chen[3]

[1]School of Electrical and Electronic Engineering, Nanyang Technological University, Singapore, [2]Department of Electronic and Information Engineering, Hong Kong Polytechnic University, Hong Kong SAR, [3]School of Electronic and Information Engineering, South China University of Technology, Guangzhou, China

Abstract An electromagnetic vector sensor consists of a triad of electric dipoles in orthogonal orientation, plus another triad of similarly arranged magnetic loops, all in spatial collocation. This electromagnetic vector sensor has been used in a series of algorithms to estimate the incident sources' directions-of-arrival and polarizations. However, these algorithms have presumed the dipole triads and the loop triads of perfect ideality in their gain/phase responses, their orientations, and locations. Such idealization is rarely (if ever) attained in actual field deployment. Instead, the nonidealities need to be calibrated, often blindly with *no* training signal impinging from any prior known direction-of-arrival at any prior known polarization. For such a scenario, this work proposes a new algorithm for direction finding, for polarization estimation, and for "blind" calibration (a.k.a. "self-calibration," "autocalibration," or "unaided calibration") of all above nonidealities. This new algorithm is *orders-of-magnitude* computationally simpler than maximum likelihood estimation. This reduction in complexity is achieved here by exploiting the electromagnetic vector sensor's quintessential array manifold and by a judicious breakdown of the originally high-dimensional problem (of estimating the directions-of-arrival, polarizations, and the antenna nonidealities) into suitably chosen/sequenced low-dimensional subproblems. This proposed algorithm is first in the open literature to exploit the electromagnetic vector-sensor's quintessential array manifold for "blind" calibration of all above mentioned nonidealities simultaneously. Monte Carlo simulations verify this proposed algorithm's effectiveness in "blind" calibration and this algorithm's *orders-of-magnitude* computational efficiency over the maximum likelihood approach.

Plain Language Summary A special kind of antenna can measure an electromagnetic wave of the wave's "deep" details. That antenna is called a "vector sensor." Like all real-world antennas, the "vector sensor" can deviate from its nominal characteristics. Those deviations are estimated here in this paper in a computationally simple way, by exploiting special properties of this "vector sensor."

1. Introduction

1.1. The Six-Component Electromagnetic Vector Sensor's *Ideal* Array Manifold

A six-component electromagnetic vector sensor is composed of three orthogonally oriented and identical dipoles that are electrically short, plus three orthogonally oriented and identical loops that are magnetically small—all collocated in a point-like spatial geometry. Such a collocated array measures all three Cartesian components of the incident electric field and all three Cartesian components of the incident magnetic field, distinctly as a 6×1 vector, at any particular spatial location and at any time instant.

The orthogonality among the three dipoles would reduce mutual coupling among them. Similarly, there would be little mutual coupling among the three orthogonal loops. Hence, the electromagnetic vector sensor's array manifold would approximately be a concatenation of the 3×1 electric field vector with the 3×1

magnetic field vector [*Nehorai and Paldi*, 1994]:

$$\mathbf{a}(\theta_k, \phi_k, \gamma_k, \eta_k) \overset{\text{def}}{=} \begin{bmatrix} \mathbf{e}(\theta_k, \phi_k, \gamma_k, \eta_k) \\ \mathbf{h}(\theta_k, \phi_k, \gamma_k, \eta_k) \end{bmatrix} \overset{\text{def}}{=} \begin{bmatrix} \cos(\phi_k)\cos(\theta_k) & -\sin(\phi_k) \\ \sin(\phi_k)\cos(\theta_k) & \cos(\phi_k) \\ -\sin(\theta_k) & 0 \\ -\sin(\phi_k) & -\cos(\phi_k)\cos(\theta_k) \\ \cos(\phi_k) & -\sin(\phi_k)\cos(\theta_k) \\ 0 & \sin(\theta_k) \end{bmatrix} \begin{bmatrix} \sin(\gamma_k)e^{j\eta_k} \\ \cos(\gamma_k) \end{bmatrix}, \tag{1}$$

where $\theta_k \in [0, \pi]$ symbolizes the kth incident source's elevation angle measured from the positive z axis, $\phi_k \in [-\pi, \pi]$ represents the corresponding azimuth angle measured from the positive x axis, $\gamma_k \in [0, \pi/2]$ denotes the auxiliary polarization angle, and $\eta_k \in [-\pi, \pi]$ refers to the polarization phase difference. Furthermore, the Frobenius norms $\|\mathbf{e}_k\| = \|\mathbf{h}_k\| = 1, \forall(\theta_k, \phi_k, \gamma_k, \eta_k)$.

The electromagnetic *vector* sensor is versatile for direction finding, because of its array manifold in (1):

1. Each electromagnetic vector sensor intrinsically offers two-dimensional azimuth-elevation directivity. Multiple incident sources' azimuth angles and elevation angles may thus be estimated and automatically matched, even with only one electromagnetic vector sensor.
2. The electromagnetic vector sensor's array manifold is free from complications from the incident source's spectrum, i.e., the incident signal's bandwidth, center frequency, and variation over time. This is due to the spatial collocation of the electromagnetic vector sensor's constituent antennas.
3. The electromagnetic vector sensor is physically compact in size, due also to the spatial collocation of its constituent dipoles and loops.

These three advantages would be unobtainable from an array of spatially displaced antennas, where the array's overall directivity depends on the frequency-dependent spatial phase factor between antennas.

For thorough surveys of dozens of algorithms that exploit the electromagnetic vector sensor's unique array manifold to estimate the incident sources' directions-of-arrival and polarizations, please see *Au-Yeung and Wong* [2009] and *Wong and Yuan* [2011]. These algorithms (except the few to be noted in section 1.2) presume the electromagnetic vector sensor(s) to have ideal gain/phase responses, perfectly known orientation(s), and perfectly known location(s)—assumptions not made in this paper.

1.2. Literature Review of Relevant Calibration Algorithms

The open literature contains many array calibration algorithms, they are not specifically tailored for the electromagnetic vector sensor (with the exception of *Lan-mei et al*. [2005, 2007], *Jia-cai et al*. [2009a, 2009b], *An-jing et al.* [2010], and *You et al.* [2010]), in the sense of *not* exploiting any uniqueness of the electromagnetic vector sensor's distinctive array manifold. As for *Lan-mei et al.* [2005, 2007] and *An-jing et al.* [2010], they affront only gain/phase uncertainties but not any misorientation nor any dislocation as in the present work. Moreover, *Lan-mei et al.* [2005, 2007] aided calibration methods requiring prior information about the incident sources, unlike the "blind" calibration in this work, whereas *An-jing et al.* [2010] unrealistically require all incident sources to have a zero elevation angle and ignore all *intra*vector sensor uncertainties. More specifically, equations (22) and (23) of *Lan-mei et al.* [2005] presume prior knowledge of the polarization phase difference. Also, *Lan-mei et al.* [2007] require the existence of two cooperating sources to incident from *one identical* direction-of-arrival *prior known* to the calibration algorithm. As for *Jia-cai et al.* [2009a, 2009b] and *You et al.* [2010], they claim to calibrate misorientation, but they use fundamentally incorrect misorientation models, in equation (2) of *Jia-cai et al.* [2009a], in equation (4) of *Jia-cai et al.* [2009b], and in equations (7) and (8) of *You et al.* [2010], such that their calibration schemes are invalid. The rotation matrices in those equations actually depend on the incident source's direction-of-arrival. Furthermore, *Jia-cai et al.* [2009a, 2009b] and *You et al.* [2010] do not calibrate any dislocation nor any gain/phase uncertainty as in this present paper. Aided calibration schemes have also been proposed for orthogonally oriented dipoles and/or loops in *Appadwedula and Keller* [2006] and *Mir and Sahr* [2007], but these schemes (unlike the present work) do not perform "blind" calibration and do not apply to the six-component electromagnetic vector sensor.

For the calibration of electromagnetic vector sensors, this present paper is first to the open literature (to the best of the present authors' knowledge) to offer any of the following:

1. To "blindly" calibrate electromagnetic vector sensors, needing no cooperating emitter of prior known arrival direction or polarization. This is with the exception of [*An-jing et al.*, 2010], which unrealistically requires all (supposedly noncooperating) emitters to have zero elevation.
2. To calibrate ("blindly" or otherwise) the *intra*electromagnetic vector sensor gain/phase uncertainties or misorientation.
3. To require no iterative search and no exhaustive search, in calibrating the electromagnetic vector sensor(s).
4. To be computationally very efficient in calibrating the electromagnetic vector sensor(s)—computationally *orders-of-magnitude* more efficient than maximum likelihood estimation. The presently proposed algorithm breaks a high-dimensional nonlinear optimization problem into several optimization problems of much lower dimensions that can be solved mostly as linear equations, thereby facilitating much faster and more probably convergence to the global optimum.

The above are achieved here via new exploitations of how the electromagnetic vector sensor's electric field/magnetic field components are interrelated quintessentially among themselves in (1). Specifically, please refer to (16) to (19) in step #3B, (22) to (25) in step #3C, (38) to (39) in step #5, and (40) in step #6. However, this proposed "blind" calibration algorithm is predicated on the availability of (possibly) uncooperative sources that are separable in frequency and in azimuth elevation.

An acoustic counterpart exists [*Song et al.*, 2014] for this proposed electromagnetic acoustic vector sensor calibration scheme. Both the electromagnetic and the acoustic schemes have parallel objectives and motif, but their array manifolds are mathematically distinct, resulting in different high-order sets of numerous parameters to be estimated and in different ways to decouple these numerous parameters.

2. The Array Manifold of a Nonideal Electromagnetic Vector Sensor, Composed of Dipole Triad/Loop Triad Subject to Unequal Gain/Phase Responses, Dislocation, Misorientation

Consider an electromagnetic vector sensor, with its dipole triad and loop triad each subject to deviations from their nominal gain/phase responses, locations, and/or orientations. The ideal array manifold of (1) would then become

$$\mathbf{a}_k^{(\ell)} = \underbrace{e^{j\frac{2\pi f_k}{c}\left(x^{(\ell)}u_k + y^{(\ell)}v_k + z^{(\ell)}w_k\right)}}_{=q_k^{(\ell)}} e^{j\frac{2\pi f_k}{c}\left\{u_k\Delta_x^{(\ell)} + v_k\Delta_y^{(\ell)} + w_k\Delta_z^{(\ell)}\right\}} \cdot \mathbf{G}\left(\mathcal{G}^{(\ell)}\right)\mathbf{P}\left(\mathcal{E}^{(\ell)}\right)\begin{bmatrix}\mathbf{e}_k^{(\ell)}\\ \mathbf{h}_k^{(\ell)}\end{bmatrix}, \tag{2}$$

where the superscript $^{(\ell)}$ identifies the ℓth electromagnetic vector sensor under discussion, * symbolizes complex conjugation, and

$$\mathbf{e}_k^{(\ell)} = \mathbf{e}\left(\theta_k^{(\ell,e)}, \phi_k^{(\ell,e)}, \gamma_k, \eta_k\right),$$
$$\mathbf{h}_k^{(\ell)} = \mathbf{h}\left(\theta_k^{(\ell,h)}, \phi_k^{(\ell,h)}, \gamma_k, \eta_k\right),$$

with $\theta_k^{(\ell,e)}$ and $\phi_k^{(\ell,e)}$ defined with respect to the ℓth dipole triad's (possibly) misoriented coordinates, and $\theta_k^{(\ell,h)}$ and $\phi_k^{(\ell,h)}$ defined with respect to the ℓth loop triad's (possibly) misoriented coordinates.

The following will discuss the individual factors in (2):

1. The *intra*vector sensor gain deviation is represented by a 6×6 diagonal matrix,

$$\mathbf{G}\left(\mathcal{G}^{(\ell)}\right) = \begin{bmatrix} g_e^{(\ell)}\mathbf{I}_3 & \mathbf{0}_3 \\ \mathbf{0}_3 & g_h^{(\ell)}\mathbf{I}_3 \end{bmatrix}, \tag{3}$$

where $\mathcal{G}^{(\ell)} = \left\{g_e^{(\ell)}, g_h^{(\ell)}\right\}$, and diag{…} denotes a diagonal matrix with the diagonal elements specified sequentially inside { }. The above idealizes each dipole triad (loop triad) to consist of dipoles (loops) of an equal gain; this assumption is not entirely unreasonable for dipoles (loops) coming in a same lot from the manufacturer. Alternatively, the above could be understood as the dipoles/loops are already calibrated/corrected in a factory/laboratory, before the electromagnetic vector sensors are deployed

in the field, because each triad is likely to have been preassembled before field deployment and unlikely to be assembled only in the field. Moreover, this above nonideality model also assumes that sufficient electromagnetic isolation has been achieved between the antennas and their support frame.

2. Each dipole triad/loop triad suffers its own phase uncertainty as a unit, independent from other vector sensors. This implicitly idealizes each dipole triad (loop triad) to consist of dipoles (loops) of an equal phase. This assumption is not entirely unreasonable for dipoles (loops) coming in a same lot from the manufacturer. So

$$\mathbf{P}\left(\mathcal{E}^{(\ell)}\right) = \begin{bmatrix} e^{j\epsilon_e^{(\ell)}}\mathbf{I}_3 & \mathbf{0}_3 \\ \mathbf{0}_3 & e^{j\epsilon_h^{(\ell)}}\mathbf{I}_3 \end{bmatrix}, \tag{4}$$

where $\mathcal{E}^{(\ell)} = \left\{\epsilon_e^{(\ell)}, \epsilon_h^{(\ell)}\right\}$, $\mathbf{I}_3$ symbolizes a 3×3 identify matrix, and $\mathbf{0}_3$ signifies a 3×3 matrix of all zeroes. At each electromagnetic vector sensor, one of its two triads would serve as a phase reference; hence, either $\epsilon_e^{(\ell)} = 0$ or $\epsilon_h^{(\ell)} = 0$, for each ℓ.

3. Each dipole triad and each loop triad may (as a unit) suffer a misorientation independent of all other triads. However, each dipole triad (loop triad) has no misorientation internally among its three dipoles (loops). The misorientation is represented by a 3×3 diagonal matrix,

$$\begin{aligned}\mathbf{R}\left(\alpha^{(\ell,\varsigma)}, \varphi^{(\ell,\varsigma)}, \psi^{(\ell,\varsigma)}\right) = &\begin{bmatrix} \cos\psi^{(\ell,\varsigma)} & \sin\psi^{(\ell,\varsigma)} & 0 \\ -\sin\psi^{(\ell,\varsigma)} & \cos\psi^{(\ell,\varsigma)} & 0 \\ 0 & 0 & 1 \end{bmatrix}\begin{bmatrix} 1 & 0 & 0 \\ 0 & \cos\varphi^{(\ell,\varsigma)} & \sin\varphi^{(\ell,\varsigma)} \\ 0 & -\sin\varphi^{(\ell,\varsigma)} & \cos\varphi^{(\ell,\varsigma)} \end{bmatrix} \\ &\cdot\begin{bmatrix} \cos\alpha^{(\ell,\varsigma)} & 0 & -\sin\alpha^{(\ell,\varsigma)} \\ 0 & 1 & 0 \\ -\sin\alpha^{(\ell,\varsigma)} & 0 & \cos\alpha^{(\ell,\varsigma)} \end{bmatrix},\end{aligned} \tag{5}$$

with $\varsigma = e$ for a dipole triad, and $\varsigma = h$ for a loop triad. The misorientation model in (5) involves three sequential rotations: (i) rotation by an angle of $\alpha^{(\ell,\varsigma)}$ around the y axis on the x-z plane, (ii) then a second rotation by an angle of $\varphi^{(\ell,\varsigma)}$ around the x axis on the y-z plane, and (iii) lastly a third rotation by an angle of $\psi^{(\ell,\varsigma)}$ around the z axis on the x-y plane.

This relates the Cartesian direction cosines $\{u_k, v_k, w_k\}$ defined with respect to the original coordinates, to $\{u_k^{(\ell,\varsigma)}, v_k^{(\ell,\varsigma)}, w_k^{(\ell,\varsigma)}\}$ defined with respect to the ℓth (possibly) dipole triad's or loop triad's misoriented coordinates. Mathematically,

$$\begin{bmatrix} u_k^{(\ell,\varsigma)} \\ v_k^{(\ell,\varsigma)} \\ w_k^{(\ell,\varsigma)} \end{bmatrix} \stackrel{\text{def}}{=} \begin{bmatrix} \sin\theta_k^{(\ell,\varsigma)}\cos\phi_k^{(\ell,\varsigma)} \\ \sin\theta_k^{(\ell,\varsigma)}\sin\phi_k^{(\ell,\varsigma)} \\ \cos\theta_k^{(\ell,\varsigma)} \end{bmatrix} = \mathbf{R}\left(\alpha^{(\ell,\varsigma)}, \varphi^{(\ell,\varsigma)}, \psi^{(\ell,\varsigma)}\right)\begin{bmatrix} u_k \\ v_k \\ w_k \end{bmatrix}. \tag{6}$$

The above (6) interrelates each incident source's Poynting vector (but *not* each source's electric field vector nor magnetic field vector) before and after any misorientation. The Appendix disproves (by a counterexample) the existence of any general transformation matrix (independent of the sources' directions-of-arrival) that can interrelate *any arbitrary* source's electric field or magnetic field, before and after *any* misorientation. Also, note that the two-step rotation is wrong in *Wong and Zoltowski* [2000] and *Wong et al.* [2004].

4. $q_k^{(\ell)}$ represents the kth source's *spatial* phase factor relating the ℓth electromagnetic vector sensor's *nominal* location $\left(x^{(\ell)}, y^{(\ell)}, z^{(\ell)}\right)$ to the reference location of $(0, 0, 0)$, with f_k denoting the kth narrowband source's center frequency, and c symbolizing the propagation speed.
5. $e^{j\frac{2\pi f_k}{c}\left\{u_k\Delta_x^{(\ell)} + v_k\Delta_y^{(\ell)} + w_k\Delta_z^{(\ell)}\right\}}$ corresponds to the kth source's spatial phase factor relating the ℓth electromagnetic vector sensor's nominal location at $\left(x^{(\ell)}, y^{(\ell)}, z^{(\ell)}\right)$ and actual location at $\left(x^{(\ell)} + \Delta_x^{(\ell)}, y^{(\ell)} + \Delta_y^{(\ell)}, z^{(\ell)} + \Delta_z^{(\ell)}\right)$. Moreover, $\Delta^{(\ell)} = \left\{\Delta_x^{(\ell)}, \Delta_y^{(\ell)}, \Delta_z^{(\ell)}\right\}$. The above model allows each electromagnetic vector sensor to be arbitrarily mislocated as a unit. However, within each electromagnetic vector sensor, individual component sensors suffer no *intra*vector sensor dislocation but remain collocated.

The above measurement model is parameterized by $12L - 7$ number of real-value unknown scalars: (a) $2L - 1$ number of real-value scalars for $2L - 1$ triads' unknown gains, (b) $6L - 3$ number of real-value scalars for $2L - 1$ triads' unknown mis-orientations, (c) $3L - 3$ number of real-value scalars for $L - 1$ electromagnetic vector-sensors' unknown dislocations, and (d) L number of real-value scalars for $L - 1$ triads' unknown phases.

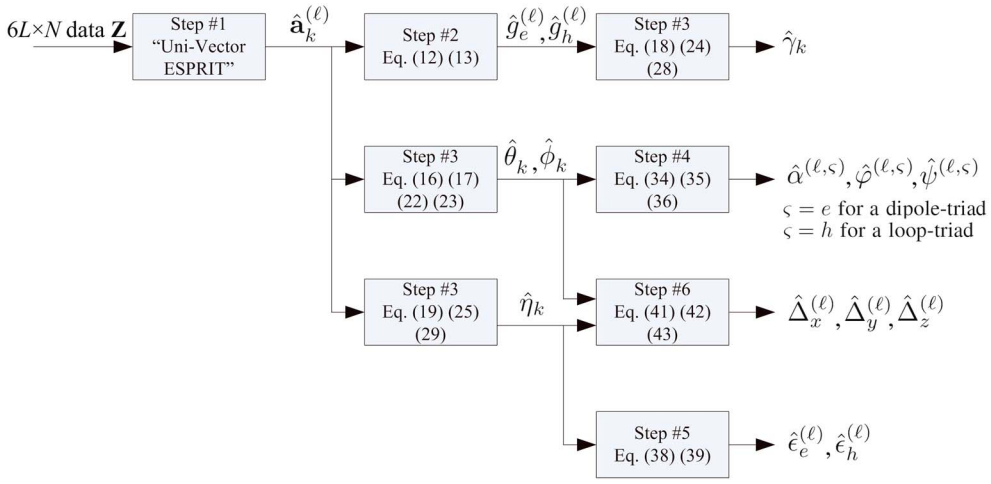

Figure 1. A flowchart outlining the logical relationships among the various steps (in sections 4–9) of the proposed "blind" calibration algorithm.

In the degenerate case of $g_e^{(\ell)} = g_h^{(\ell)} = 1$ and $\alpha^{(\ell)} = \varphi^{(\ell)} = \psi^{(\ell)} = \Delta_x^{(\ell)} = \Delta_y^{(\ell)} = \Delta_z^{(\ell)} = 0$, then the ℓth nonideal array manifold (2) would become the ideal array manifold of (1).

Of the L electromagnetic vector sensors deployed, one must serve as a reference unit, to be indexed here at $\ell = 1$ and to be located exactly at $\left(x^{(1)}, y^{(1)}, z^{(1)}\right) = (0, 0, 0)$, without loss of generality. This first electromagnetic vector sensor's dipole triad, by definition, thus suffers no mislocation (i.e., $\Delta^{(1)}$ has all zero entries). This $\ell = 1$st electromagnetic vector sensor would also have (i) *either* its dipole triad *or* its loop triad to serve as the orientational reference and (ii) *either* its dipole triad *or* its loop triad to serve as the gain reference (i.e., either $g_e^{(1)}$ or $g_h^{(1)}$ is prior known).

The subsequently proposed "blind" calibration algorithm will consist of these six steps, to be developed in details in sections 4 to 9.

Step #1. Section 4 will estimate the K noncooperating incident sources' individual steering vectors, to allow subsequent steps to exploit the electromagnetic vector sensor array manifold's unique characteristics.

Step #2. Section 5 will calibrate "blindly" each of the $2L - 1$ dipole triads'/loop triads' gain uncertainties, by exploiting the fact that each incident source's electrical field vector has the same Frobenius norm as that same source's magnetic field vector, regardless of any individual dipole triad's or loop triad's possible phase uncertainty, misorientation, or dislocation.

Step #3. Section 6 will estimate "blindly" each incident source's azimuth-elevation direction-of-arrival and polarization, by exploiting the electric field's and the magnetic field's quintessential dependence on the source's azimuth-elevation direction-of-arrival and polarization parameters.

Step #4. Section 7 will calibrate "blindly" each nonreference vector sensor's misorientation. This involves estimating $6L - 3$ unknown real-value scalars.

Step #5. Section 8 will calibrate "blindly" each of the L electromagnetic vector sensor's individual phase uncertainties, by exploiting the relationship between any vector sensor's vertically oriented dipole and vertically oriented loop.

Step #6. Section 9 will calibrate "blindly" each nonreference vector sensor's displacement from its nominal position. This involves the estimation of $3L - 3$ unknown real-value scalars, by exploiting the relationship between that vector sensor's vertically oriented dipole and vertically oriented loop.

Figure 1 shows the logical sequence among these steps in a flowchart.

For each step, the minimum required number of sources is 3, but there is no ceiling for the maximum allowable number of sources—as will be explained later. This three-source minimum is often not a problem:

1. In military environments, several radar/jamming systems are often used to simultaneously cover several spatial regions and/or several frequency bands.

2. In civilian environments, many "sources of opportunity" would likely exist, e.g., radio, TV, and mobiles.
3. In emergency rescue situations, several people trapped in a building/mine/avalanche might each have an active beacon.

3. Statistical Data Model

Let there be $K \geq 3$ number of incident sources. At the ℓth electromagnetic vector sensor, the following 6×1 data vector is received at time t:

$$\mathbf{z}^{(\ell)}(t) = \sum_{k=1}^{K} \mathbf{a}_k^{(\ell)} s_k(t) + \mathbf{n}(t). \tag{7}$$

The kth signal is a pure tone $s_k(t) = \sqrt{\mathcal{P}_k} e^{j(2\pi f_k t + \varphi_k)}$, at frequency f_k, distinct from the other $K-1$ frequencies. Also, T_s symbolizes the a priori known time-sampling period. The proposed algorithm also works for narrowband signals having nonzero bandwidths, if each signal has a prior known subband wherein only that signal exists. Moreover, $\mathcal{P}_k$ denotes the signal power (a priori unknown to the receiver); φ_k signifies a random phase (uncorrelated to all other random entities). It is further assumed that $(\theta_k, \phi_k) \neq (\theta_j, \phi_j), \forall k \neq j \in \{1, \ldots, K\}$. The additive noise $\mathbf{n}(t)$ is modeled as zero mean, spatiotemporally uncorrelated, with (a priori unknown) power $\mathcal{P}_N$.

The present calibration problem aims to estimate all earlier mentioned array manifold nonideality parameters plus the sources' arrival angles, given the $6L \times N$ collected data $\mathbf{Z} = \left[\mathbf{z}(T_s), \mathbf{z}(2T_s), \ldots, \mathbf{z}(NT_s)\right]$, where $\mathbf{z}(t) = \left[\left(\mathbf{z}^{(1)}(t)\right)^T, \ldots, \left(\mathbf{z}^{(L)}(t)\right)^T\right]^T$, and $N > 12L+1$. For a justification of the last inequality, please refer to *Wong and Zoltowski* [1997].

This data model involves the $12L - 7$ real-value unknown scalars listed previously in section 2, plus these $4K$ real-value unknown scalars: (e) $2K$ number of real-value scalars for the K sources' unknown directions-of-arrival and (f) $2K$ number of real-value scalars for the K sources' unknown polarization parameters.

On the other hand, there exists $6KL$ number of constraints from the $6KL$ real-value scalar measurements at any time instant. For a unique estimation of the directions-of-arrival, polarization parameters and the nonideality parameters, the $6KL$ number of real-value constraints $6KL$ must not be less than the $12L + 4K - 7$ number of real-value unknown scalars. That is,

$$K \geq \frac{1}{2}\frac{12L-7}{3L-2} \qquad \Rightarrow \qquad K \geq 3, \text{ for any } L. \tag{8}$$

The above equality compares the number of nonlinear constraints versus the number of unknown scalars, by considering all L electromagnetic vector sensors as a whole. With respect to the individual steps (mentioned at the end of section 2) of the presently proposed algorithm, only $K \geq 1$ is needed (regardless of L) to estimate gain uncertainties and phase uncertainties, whereas $K \geq 3$ is needed (regardless of L) to estimate misorientations and mislocations due to these estimation problems' intrinsically trivariate parametric nature (but not due to the specific estimation algorithms herein proposed). With more (separable) signals, the data could yield more (nonlinear) constraints to estimate each electromagnetic vector sensor's nonideal parameters, as well as to estimate each source's direction-of-arrival and polarization.

4. Proposed Algorithm's Step #1: Estimation of Each Source's Steering Vector

This step will estimate each incident source's steering vector $\{\mathbf{a}_k, \forall k = 1, 2, \ldots, K\}$, to within an (unknown) complex-value constant. Here $\mathbf{a}_k = \left[\left(\mathbf{a}_k^{(1)}\right)^T, \ldots, \left(\mathbf{a}_k^{(L)}\right)^T\right]^T$ stacks all L electromagnetic vector sensors' individual 6×1 steering vectors in (2), to give the entire array's $6L \times 1$ steering vectors. The steering vector estimates ($\hat{\mathbf{a}}_1, \ldots, \hat{\mathbf{a}}_K$, which will be defined later) would allow subsequent sections to exploit the salient attributes of the electromagnetic vector sensor array manifold for "blind" calibration.

For the "multiple pure tone" signal model in section 3 the "Uni-Vector-Sensor ESPRIT" algorithm [*Wong and Zoltowski*, 1997] may be used. That algorithm exploits the pure tones' temporal "invariance" over the sampling instants $\{T_s, 2T_s, \ldots, NT_s\}$. The following will summarize the algorithmic steps of the *Uni-Vector-Sensor ESPRIT* algorithm. For the motivations underlying these algorithmic steps, please refer to the lengthy exposition in *Wong and Zoltowski* [1997] itself.

1. Form the data matrices,

$$\mathbf{Z}_1 = \left[\mathbf{z}(T_s), \mathbf{z}(2T_s), \ldots, \mathbf{z}(NT_s - \Delta_T)\right],$$
$$\mathbf{Z}_2 = \left[\mathbf{z}(T_s + \Delta_T), \mathbf{z}(2T_s + \Delta_T), \ldots, \mathbf{z}(NT_s)\right],$$

   where Δ_T equals some nonzero integer multiple of T_s. Then, form the data matrix $\mathbf{Z} = [\mathbf{Z}_1^T, \mathbf{Z}_2^T]^T$.
2. Eigen-decompose $\mathbf{Z}\mathbf{Z}^H$, such that $\mathbf{E}_s = [\mathbf{E}_1^T, \mathbf{E}_2^T]^T$ represents the $12L \times K$ matrix (the signal-subspace eigenvector matrix) whose K columns equal the K principal eigenvectors associated with the K largest-magnitude eigenvalues. Here the superscript ^{H} symbolizes the Hermitian operator.
3. Define the $K \times K$ matrix, $\mathbf{\Psi} \overset{\text{def}}{=} \left(\mathbf{E}_1^H\mathbf{E}_1\right)^{-1}\left(\mathbf{E}_1^H\mathbf{E}_2\right) = \mathbf{T}^{-1}\mathbf{\Phi}\mathbf{T}$, where the kth eigenvalue of $\mathbf{\Psi}$ equals $[\mathbf{\Phi}]_{k,k} = e^{j2\pi f_k \Delta_T}, \forall k = 1, \ldots, K$, and the corresponding right-eigenvector constitutes the jth column of $\mathbf{T}$.
4. The K impinging sources' steering vectors may be estimated, each to within a complex-value multiplicative scalar, as $\left[\hat{\mathbf{a}}_1, \ldots, \hat{\mathbf{a}}_K\right] = \frac{1}{2}\left\{\mathbf{E}_1\mathbf{T}^{-1} + \mathbf{E}_2\mathbf{T}^{-1}\mathbf{\Phi}^{-1}\right\} \approx \left[c_1\mathbf{a}_1, \ldots, c_K\mathbf{a}_K\right]$. These K *unknown* complex-value multiplicative scalars arise from the eigen-decomposition of $\mathbf{\Psi}$.

Alternatively, if $\{f_k, \forall k\}$ is prior known, a band-pass filter could then be constructed to separate each pure tone from all other pure tones.

For the narrowband data model, in which signals have disjoint nonzero bandwidths, skip Step #1 here in section 4. Instead, comb-filtering could be applied to each sensor's raw data in order to isolate each signal at its prior known subband. This will produce a $6L \times N$ matrix $\mathbf{Z}_k$. To alleviate the additive noise's adverse effects, eigen-decompose $\mathbf{Z}_k^H\mathbf{Z}_k$ to obtain its principal eigenvector $\hat{\mathbf{a}}_k \approx c_k\mathbf{a}_k$, where c_k represents an unknown complex-value scalar. Many other methods exist [e.g., *Belouchrani et al.*, 1997].

This Step #1 has isolated each noncooperating source's steering vector, to allow subsequent steps to exploit the electromagnetic vector sensor array manifold's unique characteristics.

5. Proposed Algorithm's Step #2: "Blind" Calibration of Each Vector Sensor's Gain Uncertainties

Step #2 here will now exploit the fact that (for each source and at each electromagnetic vector sensor) the electrical field vector's Frobenius norm must equal the magnetic field vector's Frobenius norm, i.e., $\left\|\mathbf{e}_k^{(\ell)}\right\| = \left\|\mathbf{h}_k^{(\ell)}\right\| = 1, \forall\theta_k, \phi_k, \gamma_k, \eta_k$, regardless of the ℓth dipole triad/loop triad's any phase uncertainty, misorientation, or dislocation, which will be calibrated, but later. This fact of $\left\|\mathbf{e}_k^{(\ell)}\right\| = \left\|\mathbf{h}_k^{(\ell)}\right\| = 1, \forall\theta_k, \phi_k, \gamma_k, \eta_k$ has also been exploited in the aided scheme in *Lan-mei et al.* [2005] to calibrate gain uncertainties.

Step #1 has computed

$$\hat{\mathbf{a}}_k^{(\ell)} \approx c_k\,\mathbf{G}\left(\mathcal{G}^{(\ell)}\right)\mathbf{P}\left(\mathcal{P}^{(\ell)}\right)\begin{bmatrix}\mathbf{e}_k^{(\ell)}\\ \mathbf{h}_k^{(\ell)}\end{bmatrix} q_k^{(\ell)} e^{j\frac{2\pi f_k}{c}\left\{u_k\Delta_x^{(\ell)} + v_k\Delta_y^{(\ell)} + w_k\Delta_z^{(\ell)}\right\}}, \forall k, \tag{9}$$

with the above approximations due to the noises in the data model. From the *intra*vector sensor gain uncertainty model in (4), it holds that

$$\frac{\left|\left[\hat{\mathbf{a}}_k^{(\ell)}\right]_1\right|^2 + \left|\left[\hat{\mathbf{a}}_k^{(\ell)}\right]_2\right|^2 + \left|\left[\hat{\mathbf{a}}_k^{(\ell)}\right]_3\right|^2}{\left(g_e^{(\ell)}\right)^2} = \frac{\left|\left[\hat{\mathbf{a}}_k^{(\ell)}\right]_4\right|^2 + \left|\left[\hat{\mathbf{a}}_k^{(\ell)}\right]_5\right|^2 + \left|\left[\hat{\mathbf{a}}_k^{(\ell)}\right]_6\right|^2}{\left(g_h^{(\ell)}\right)^2} = |c_k|^2, \forall k. \tag{10}$$

The above (10) holds $\forall k, \forall\ell$, that is, for all K incident sources and at every electromagnetic vector sensor.

Recall that the $\ell = 1$st vector sensor has one of its two triads serving as a gain reference. Therefore, $\{|c_k|^2,\ k = 1, \ldots, K\}$ may all be evaluated at $\ell = 1$ as follows:

$$\widehat{|c_k|} = \begin{cases} \frac{1}{g_e^{(1)}} \left(\left| \left[\hat{\mathbf{a}}_k^{(1)} \right]_1 \right|^2 + \left| \left[\hat{\mathbf{a}}_k^{(1)} \right]_2 \right|^2 + \left| \left[\hat{\mathbf{a}}_k^{(1)} \right]_3 \right|^2 \right)^{1/2}, & \text{if } g_e^{(1)} \text{is prior known,} \\ \frac{1}{g_h^{(1)}} \left(\left| \left[\hat{\mathbf{a}}_k^{(1)} \right]_4 \right|^2 + \left| \left[\hat{\mathbf{a}}_k^{(1)} \right]_5 \right|^2 + \left| \left[\hat{\mathbf{a}}_k^{(1)} \right]_6 \right|^2 \right)^{1/2}, & \text{if } g_h^{(1)} \text{is prior known.} \end{cases} \tag{11}$$

Substituting $\widehat{|c_k|}$ of (11) for $|c_k|$ of (10) for $k = 1, 2, \ldots, K$, the ℓth vector sensor's gain uncertainties may be estimated as

$$\hat{g}_e^{(\ell)} = \frac{1}{K} \sum_{k=1}^{K} \frac{1}{\widehat{|c_k|}} \left(\left| \left[\hat{\mathbf{a}}_k^{(\ell)} \right]_1 \right|^2 + \left| \left[\hat{\mathbf{a}}_k^{(\ell)} \right]_2 \right|^2 + \left| \left[\hat{\mathbf{a}}_k^{(\ell)} \right]_3 \right|^2 \right)^{1/2}, \tag{12}$$

$$\hat{g}_h^{(\ell)} = \frac{1}{K} \sum_{k=1}^{K} \frac{1}{\widehat{|c_k|}} \left(\left| \left[\hat{\mathbf{a}}_k^{(\ell)} \right]_4 \right|^2 + \left| \left[\hat{\mathbf{a}}_k^{(\ell)} \right]_5 \right|^2 + \left| \left[\hat{\mathbf{a}}_k^{(\ell)} \right]_6 \right|^2 \right)^{1/2}. \tag{13}$$

The above has implicitly exploited the facts that the same c_k affects all L steering vector estimates in $\left\{ \hat{\mathbf{a}}_k^{(\ell)}, \forall \ell \right\}$ and that the gain uncertainties may be calibrated without knowing $\angle c_k$, which symbolizes the angle of the complex-value scalar c_k.

6. Proposed Algorithm's Step #3: Estimation of Each Incident Source's Azimuth-Elevation Direction-of-Arrival and Polarization parameters

Though each dipole triad and each loop triad suffers its own individual misorientation, it is nevertheless possible to perform direction finding and polarization estimation using either a single dipole triad or a single loop triad, as in *Wong* [2001] and *Yuan et al.* [2012].

6.1. Preliminary Computations to Estimate sgn $\{\sin(\eta_k)\}$

The estimation method in *Wong* [2001] and *Yuan et al.* [2012] requires prior knowledge of the sign of η_k, which is allowed to be a priori *un*known in the present data model. This section 6.1 will thus estimate this $\text{sgn}(\eta_k)$, $\forall k$.

If dipole triad in the $\ell = 1$st electromagnetic vector sensor serves as the orientational reference:

$$\widehat{\text{sgn}}\left\{\sin(\eta_k)\right\} < 0, \text{ if } \begin{cases} \left\{ \Im \left(\left[\hat{\mathbf{a}}_k^{(1)} e^{-j\angle\left[-\hat{\mathbf{a}}_k^{(1)}\right]_3} \right]_2 \right) > 0 \text{ and } \phi_k \in \left[-\pi/2, \pi/2\right] \right\}, \text{or} \\ \left\{ \Im \left(\left[\hat{\mathbf{a}}_k^{(1)} e^{-j\angle\left[-\hat{\mathbf{a}}_k^{(1)}\right]_3} \right]_2 \right) < 0 \text{ and } \phi_k \in \left[-\pi, -\pi/2\right) \cup \left(\pi/2, \pi\right] \right\}, \end{cases}$$

$$\widehat{\text{sgn}}\left\{\sin(\eta_k)\right\} > 0, \text{ if } \begin{cases} \left\{ \Im \left(\left[\hat{\mathbf{a}}_k^{(1)} e^{-j\angle\left[-\hat{\mathbf{a}}_k^{(1)}\right]_3} \right]_2 \right) < 0 \text{ and } \phi_k \in \left[-\pi/2, \pi/2\right] \right\}, \text{ or} \\ \left\{ \Im \left(\left[\hat{\mathbf{a}}_k^{(1)} e^{-j\angle\left[-\hat{\mathbf{a}}_k^{(1)}\right]_3} \right]_2 \right) > 0 \text{ and } \phi_k \in \left[-\pi, -\pi/2\right) \cup \left(\pi/2, \pi\right] \right\}, \end{cases}$$

where $\Im(\cdot)$ refers to the imaginary value part of the scalar inside the parentheses.

If loop triad in the $\ell = 1$st electromagnetic vector sensor serves as the orientational reference:

$$\widehat{\text{sgn}}\left\{\sin(\eta_k)\right\} < 0, \text{ if } \begin{cases} \left\{ \Im \left(\left[\hat{\mathbf{a}}_k^{(1)} e^{-j\angle\left[\hat{\mathbf{a}}_k^{(1)}\right]_6} \right]_5 \right) < 0 \text{ and } \phi_k \in \left[-\pi/2, \pi/2\right] \right\}, \text{ or} \\ \left\{ \Im \left(\left[\hat{\mathbf{a}}_k^{(1)} e^{-j\angle\left[\hat{\mathbf{a}}_k^{(1)}\right]_6} \right]_5 \right) > 0 \text{ and } \phi_k \in \left[-\pi, -\pi/2\right) \cup \left(\pi/2, \pi\right] \right\}, \end{cases}$$

$$\widehat{\text{sgn}}\left\{\sin(\eta_k)\right\} > 0, \text{ if } \begin{cases} \left\{ \Im \left(\left[\hat{\mathbf{a}}_k^{(1)} e^{-j\angle\left[\hat{\mathbf{a}}_k^{(1)}\right]_6} \right]_5 \right) > 0 \text{ and } \phi_k \in \left[-\pi/2, \pi/2\right] \right\}, \text{ or} \\ \left\{ \Im \left(\left[\hat{\mathbf{a}}_k^{(1)} e^{-j\angle\left[\hat{\mathbf{a}}_k^{(1)}\right]_6} \right]_5 \right) < 0 \text{ and } \phi_k \in \left[-\pi, -\pi/2\right) \cup \left(\pi/2, \pi\right] \right\}. \end{cases}$$

6.2. Considering Only the ℓth Dipole Triad

Substituting (1) into (2), and then considering only the top three elements in the vector equation,

$$\begin{bmatrix}\begin{bmatrix}\hat{\mathbf{a}}_k^{(\ell)}\\ \hat{\mathbf{a}}_k^{(\ell)}\\ \hat{\mathbf{a}}_k^{(\ell)}\end{bmatrix}_1\\ \begin{bmatrix}\hat{\mathbf{a}}_k^{(\ell)}\\ \hat{\mathbf{a}}_k^{(\ell)}\\ \hat{\mathbf{a}}_k^{(\ell)}\end{bmatrix}_2\\ \begin{bmatrix}\hat{\mathbf{a}}_k^{(\ell)}\\ \hat{\mathbf{a}}_k^{(\ell)}\\ \hat{\mathbf{a}}_k^{(\ell)}\end{bmatrix}_3\end{bmatrix} \approx c_k\, g_e^{(\ell)}\, e^{j\epsilon_e^{(\ell)}}\, e^{j\frac{2\pi f_k}{c}\left\{\left(x^{(\ell)}+\Delta_x^{(\ell)}\right)u_k+\left(y^{(\ell)}+\Delta_y^{(\ell)}\right)v_k+\left(z^{(\ell)}+\Delta_z^{(\ell)}\right)w_k\right\}} \cdot \underbrace{\begin{bmatrix}\sin\gamma_k\cos\theta_k^{(\ell,e)}\cos\phi_k^{(\ell,e)}e^{j\eta_k}-\cos\gamma_k\sin\phi_k^{(\ell,e)}\\ \sin\gamma_k\cos\theta_k^{(\ell,e)}\sin\phi_k^{(\ell,e)}e^{j\eta_k}+\cos\gamma_k\cos\phi_k^{(\ell,e)}\\ -\sin\gamma_k\sin\theta_k^{(\ell,e)}e^{j\eta_k}\end{bmatrix}}_{=\mathbf{e}_k^{(\ell)}}. \tag{14}$$

The above approximation would become equality, if there were no noise or if any infinite number of snapshots were available.

To eliminate the complex phase from the third element in the vector on the left side,

$$\begin{aligned}\begin{bmatrix}\left[\hat{\mathbf{a}}_k^{(\ell)}\right]_1 e^{-j\angle\left[-\hat{\mathbf{a}}_k^{(\ell)}\right]_3}\\ \left[\hat{\mathbf{a}}_k^{(\ell)}\right]_2 e^{-j\angle\left[-\hat{\mathbf{a}}_k^{(\ell)}\right]_3}\\ \left[\hat{\mathbf{a}}_k^{(\ell)}\right]_3 e^{-j\angle\left[-\hat{\mathbf{a}}_k^{(\ell)}\right]_3}\end{bmatrix} &= |c_k|\, g_e^{(\ell)}\begin{bmatrix}\sin\gamma_k\cos\theta_k^{(\ell,e)}\cos\phi_k^{(\ell,e)}-\cos\gamma_k\sin\phi_k^{(\ell,e)}e^{-j\eta_k}\\ \sin\gamma_k\cos\theta_k^{(\ell,e)}\sin\phi_k^{(\ell,e)}+\cos\gamma_k\cos\phi_k^{(\ell,e)}e^{-j\eta_k}\\ -\sin\gamma_k\sin\theta_k^{(\ell,e)}\end{bmatrix}\\ &= |c_k|\, g_e^{(\ell)}\begin{bmatrix}\sin\gamma_k\cos\theta_k^{(\ell,e)}\cos\phi_k^{(\ell,e)}-\cos\gamma_k\sin\phi_k^{(\ell,e)}\cos\eta_k\\ \sin\gamma_k\cos\theta_k^{(\ell,e)}\sin\phi_k^{(\ell,e)}+\cos\gamma_k\cos\phi_k^{(\ell,e)}\cos\eta_k\\ -\sin\gamma_k\sin\theta_k^{(\ell,e)}\end{bmatrix}\\ &\quad + j\,|c_k|\, g_e^{(\ell)}\begin{bmatrix}\cos\gamma_k\sin\phi_k^{(\ell,e)}\sin\eta_k\\ -\cos\gamma_k\cos\phi_k^{(\ell,e)}\sin\eta_k\\ 0\end{bmatrix}.\end{aligned} \tag{15}$$

The kth source's azimuth arrival angle $\phi_k^{(\ell,e)}$ has a support range of $[-\pi,\pi)$, which may be segmented into three disjoint subranges:

1.

$$\phi_k^{(\ell,e)}\in\left[-\frac{\pi}{2},-\frac{\pi}{2}\right] \Leftrightarrow \cos\phi_k^{(\ell,e)}>0 \Leftrightarrow \widehat{\mathrm{sgn}}\left\{\sin(\eta_k)\right\}\Im\left\{\left[\hat{\mathbf{a}}_k^{(\ell)}e^{-j\angle\left[-\hat{\mathbf{a}}_k^{(\ell)}\right]_3}\right]_2\right\}<0,$$

2.

$$\begin{aligned}\phi_k^{(\ell,e)}\in\left(\frac{\pi}{2},\pi\right] &\Leftrightarrow \cos\phi_k^{(\ell,e)}<0 \text{ and } \sin\phi_k^{(\ell,e)}>0 \Leftrightarrow \widehat{\mathrm{sgn}}\left\{\sin(\eta_k)\right\}\Im\left\{\left[\hat{\mathbf{a}}_k^{(\ell)}e^{-j\angle\left[-\hat{\mathbf{a}}_k^{(\ell)}\right]_3}\right]_2\right\}\\ &>0,\ \widehat{\mathrm{sgn}}\left\{\sin(\eta_k)\right\}\Im\left\{\left[\hat{\mathbf{a}}_k^{(\ell)}e^{-j\angle\left[-\hat{\mathbf{a}}_k^{(\ell)}\right]_3}\right]_1\right\}>0,\end{aligned}$$

3.

$$\begin{aligned}\phi_k^{(\ell,e)}\in\left[-\pi,-\frac{\pi}{2}\right) &\Leftrightarrow \cos\phi_k^{(\ell,e)}<0 \text{ and } \sin\phi_k^{(\ell,e)}<0 \Leftrightarrow \widehat{\mathrm{sgn}}\left\{\sin(\eta_k)\right\}\Im\left\{\left[\hat{\mathbf{a}}_k^{(\ell)}e^{-j\angle\left[-\hat{\mathbf{a}}_k^{(\ell)}\right]_3}\right]_2\right\}\\ &>0,\ \widehat{\mathrm{sgn}}\left\{\sin(\eta_k)\right\}\Im\left\{\left[\hat{\mathbf{a}}_k^{(\ell)}e^{-j\angle\left[-\hat{\mathbf{a}}_k^{(\ell)}\right]_3}\right]_1\right\}<0,\end{aligned}$$

where $\Im\{\dot{}\}$ symbolizes the imaginary part of the entity inside the curly brackets. Then, straightforward manipulations of (15) yield (16) (please see equation (52) in *He and Liu* [2009], or Composition 1.1 in Table 1

of *Yuan et al.* [2012]). Some similar but mistaken expression appears in equation (4) of *Wong* [2001].

$$\hat{\phi}_k^{(\ell,e)} = \begin{cases} \arctan\left(-\dfrac{\Im\left\{\left[\hat{\mathbf{a}}_k^{(\ell)} e^{-j\angle\left[-\hat{\mathbf{a}}_k^{(\ell)}\right]_3}\right]_1\right\}}{\Im\left\{\left[\hat{\mathbf{a}}_k^{(\ell)} e^{-j\angle\left[-\hat{\mathbf{a}}_k^{(\ell)}\right]_3}\right]_2\right\}}\right), & \text{if } \widehat{\text{sgn}}\left\{\sin(\eta_k)\right\} \Im\left\{\left[\hat{\mathbf{a}}_k^{(\ell)} e^{-j\angle\left[-\hat{\mathbf{a}}_k^{(\ell)}\right]_3}\right]_2\right\} < 0, \\ \pi + \arctan\left(-\dfrac{\Im\left\{\left[\hat{\mathbf{a}}_k^{(\ell)} e^{-j\angle\left[-\hat{\mathbf{a}}_k^{(\ell)}\right]_3}\right]_1\right\}}{\Im\left\{\left[\hat{\mathbf{a}}_k^{(\ell)} e^{-j\angle\left[-\hat{\mathbf{a}}_k^{(\ell)}\right]_3}\right]_2\right\}}\right), & \text{if } \begin{array}{l} \widehat{\text{sgn}}\left\{\sin(\eta_k)\right\} \Im\left\{\left[\hat{\mathbf{a}}_k^{(\ell)} e^{-j\angle\left[-\hat{\mathbf{a}}_k^{(\ell)}\right]_3}\right]_2\right\} > 0, \text{and} \\ \widehat{\text{sgn}}\left\{\sin(\eta_k)\right\} \Im\left\{\left[\hat{\mathbf{a}}_k^{(\ell)} e^{-j\angle\left[-\hat{\mathbf{a}}_k^{(\ell)}\right]_3}\right]_1\right\} > 0 \end{array} \\ -\pi + \arctan\left(-\dfrac{\Im\left\{\left[\hat{\mathbf{a}}_k^{(\ell)} e^{-j\angle\left[-\hat{\mathbf{a}}_k^{(\ell)}\right]_3}\right]_1\right\}}{\Im\left\{\left[\hat{\mathbf{a}}_k^{(\ell)} e^{-j\angle\left[-\hat{\mathbf{a}}_k^{(\ell)}\right]_3}\right]_2\right\}}\right), & \text{if } \begin{array}{l} \widehat{\text{sgn}}\left\{\sin(\eta_k)\right\} \Im\left\{\left[\hat{\mathbf{a}}_k^{(\ell)} e^{-j\angle\left[-\hat{\mathbf{a}}_k^{(\ell)}\right]_3}\right]_2\right\} > 0, \text{and} \\ \widehat{\text{sgn}}\left\{\sin(\eta_k)\right\} \Im\left\{\left[\hat{\mathbf{a}}_k^{(\ell)} e^{-j\angle\left[-\hat{\mathbf{a}}_k^{(\ell)}\right]_3}\right]_1\right\} < 0 \end{array} \end{cases}. \tag{16}$$

$$\hat{\theta}_k^{(\ell,e)} = \begin{cases} \arctan\left\{\left|\dfrac{\left[\hat{\mathbf{a}}_k^{(\ell)}\right]_3}{\Re\left\{\left[\hat{\mathbf{a}}_k^{(\ell)}\right]_1 e^{-j\angle\left[-\hat{\mathbf{a}}_k^{(\ell)}\right]_3}\right\}\cos\hat{\phi}_k^{(\ell,e)} + \Re\left\{\left[\hat{\mathbf{a}}_k^{(\ell)}\right]_2 e^{-j\angle\left[-\hat{\mathbf{a}}_k^{(\ell)}\right]_3}\right\}\sin\hat{\phi}_k^{(\ell,e)}}\right|\right\}, \\ \quad \text{if } \Re\left\{\left[\hat{\mathbf{a}}_k^{(\ell)}\right]_1 e^{-j\angle\left[-\hat{\mathbf{a}}_k^{(\ell)}\right]_3}\right\}\cos\hat{\phi}_k^{(\ell,e)} + \Re\left\{\left[\hat{\mathbf{a}}_k^{(\ell)}\right]_2 e^{-j\angle\left[-\hat{\mathbf{a}}_k^{(\ell)}\right]_3}\right\}\sin\hat{\phi}_k^{(\ell,e)} > 0, \\ \pi + \arctan\left\{\left|\dfrac{\left[\hat{\mathbf{a}}_k^{(\ell)}\right]_3}{\Re\left\{\left[\hat{\mathbf{a}}_k^{(\ell)}\right]_1 e^{-j\angle\left[-\hat{\mathbf{a}}_k^{(\ell)}\right]_3}\right\}\cos\hat{\phi}_k^{(\ell,e)} + \Re\left\{\left[\hat{\mathbf{a}}_k^{(\ell)}\right]_2 e^{-j\angle\left[-\hat{\mathbf{a}}_k^{(\ell)}\right]_3}\right\}\sin\hat{\phi}_k^{(\ell,e)}}\right|\right\}, \\ \quad \text{if } \Re\left\{\left[\hat{\mathbf{a}}_k^{(\ell)}\right]_1 e^{-j\angle\left[-\hat{\mathbf{a}}_k^{(\ell)}\right]_3}\right\}\cos\hat{\phi}_k^{(\ell,e)} + \Re\left\{\left[\hat{\mathbf{a}}_k^{(\ell)}\right]_2 e^{-j\angle\left[-\hat{\mathbf{a}}_k^{(\ell)}\right]_3}\right\}\sin\hat{\phi}_k^{(\ell,e)} < 0, \end{cases} \tag{17}$$

The elevation arrival angle $\theta_k^{(\ell,e)}$ has a support range of $[0, \pi]$, which may be segmented into two disjoint subranges:

1.
$$\theta_k^{(\ell,e)} \in \left[0, \frac{\pi}{2}\right) \Leftrightarrow \cos\theta_k^{(\ell,e)} > 0 \Leftrightarrow \Re\left\{\left[\hat{\mathbf{a}}_k^{(\ell)}\right]_1 e^{-j\angle\left[-\hat{\mathbf{a}}_k^{(\ell)}\right]_3}\right\}\cos\hat{\phi}_k^{(\ell,e)} + \Re\left\{\left[\hat{\mathbf{a}}_k^{(\ell)}\right]_2 e^{-j\angle\left[-\hat{\mathbf{a}}_k^{(\ell)}\right]_3}\right\}\sin\hat{\phi}_k^{(\ell,e)} > 0,$$

2.
$$\theta_k^{(\ell,e)} \in \left[\frac{\pi}{2}, \pi\right] \Leftrightarrow \cos\theta_k^{(\ell,e)} < 0 \Leftrightarrow \Re\left\{\left[\hat{\mathbf{a}}_k^{(\ell)}\right]_1 e^{-j\angle\left[-\hat{\mathbf{a}}_k^{(\ell)}\right]_3}\right\}\cos\hat{\phi}_k^{(\ell,e)} + \Re\left\{\left[\hat{\mathbf{a}}_k^{(\ell)}\right]_2 e^{-j\angle\left[-\hat{\mathbf{a}}_k^{(\ell)}\right]_3}\right\}\sin\hat{\phi}_k^{(\ell,e)} < 0,$$

where $\Re\{\cdot\}$ denotes real-value part of the entity inside the curly brackets. Then, straightforward manipulations of (15) yield (17) (please see equation (53) in *He and Liu* [2009], or Composition 1.1 in Table 1 of *Yuan et al.* [2012]). Some similar but mistaken expression appears in equation (5) of *Wong* [2001].

Based on equations (6) and (7) in *Wong* [2001], equations (54) and (55) in *He and Liu* [2009], or Composition 1.1 in Table 1 of *Yuan et al.* [2012],

$$\hat{\gamma}_k^{(\ell,e)} = \arcsin\left|\frac{1}{\hat{g}_e^{(\ell)}} \frac{\left[\hat{\mathbf{a}}_k^{(\ell)}\right]_3 / |c_k|}{\sin\hat{\theta}_k^{(\ell,e)}}\right|, \tag{18}$$

$$\hat{\eta}_k^{(\ell,e)} = -\angle\left(\left[\hat{\mathbf{a}}_k^{(\ell)} e^{-j\angle\left[-\hat{\mathbf{a}}_k^{(\ell)}\right]_3}\right]_2 \cos\hat{\phi}_k^{(\ell,e)} - \left[\hat{\mathbf{a}}_k^{(\ell)} e^{-j\angle\left[-\hat{\mathbf{a}}_k^{(\ell)}\right]_3}\right]_1 \sin\hat{\phi}_k^{(\ell,e)}\right). \tag{19}$$

Note that the above estimation for $\{\hat{\theta}_k^{(\ell,e)}, \hat{\phi}_k^{(\ell,e)}, \hat{\eta}_k^{(\ell,e)}\}$ in (17)–(19) is *in*dependent of the gain uncertainties and the a priori unknown complex-value scalar c_k.

6.3. Considering Only the ℓth Loop Triad

Substituting again (1) into (2), but now considering only the bottom three elements in the vector equation,

$$\begin{bmatrix} \left[\hat{\mathbf{a}}_k^{(\ell)}\right]_4 \\ \left[\hat{\mathbf{a}}_k^{(\ell)}\right]_5 \\ \left[\hat{\mathbf{a}}_k^{(\ell)}\right]_6 \end{bmatrix} \approx c_k\, g_h^{(\ell)}\, e^{j\epsilon_h^{(\ell)}}\, e^{j\frac{2\pi f_k}{c}\left\{(x^{(\ell)}+\Delta_x^{(\ell)})u_k+(y^{(\ell)}+\Delta_y^{(\ell)})v_k+(z^{(\ell)}+\Delta_z^{(\ell)})w_k\right\}} \underbrace{\begin{bmatrix} -\sin\gamma_k \sin\phi_k^{(\ell,h)} e^{j\eta_k} - \cos\gamma_k \cos\theta_k^{(\ell,h)} \cos\phi_k^{(\ell,h)} \\ \sin\gamma_k \cos\phi_k^{(\ell,h)} e^{j\eta_k} - \cos\gamma_k \cos\theta_k^{(\ell,h)} \sin\phi_k^{(\ell,h)} \\ \cos\gamma_k \sin\theta_k^{(\ell,h)} \end{bmatrix}}_{=\mathbf{h}_k^{(\ell)}}. \tag{20}$$

To eliminate the phase in the third element of the vector

$$\begin{aligned} \begin{bmatrix} \left[\hat{\mathbf{a}}_k^{(\ell)}\right]_4 e^{-j\angle\left[\hat{\mathbf{a}}_k^{(\ell)}\right]_6} \\ \left[\hat{\mathbf{a}}_k^{(\ell)}\right]_5 e^{-j\angle\left[\hat{\mathbf{a}}_k^{(\ell)}\right]_6} \\ \left[\hat{\mathbf{a}}_k^{(\ell)}\right]_6 e^{-j\angle\left[\hat{\mathbf{a}}_k^{(\ell)}\right]_6} \end{bmatrix} &= |c_k|\, g_h^{(\ell)} \begin{bmatrix} -\sin\gamma_k \sin\phi_k^{(\ell,h)} e^{j\eta_k} - \cos\gamma_k \cos\theta_k^{(\ell,h)} \cos\phi_k^{(\ell,h)} \\ \sin\gamma_k \cos\phi_k^{(\ell,h)} e^{j\eta_k} - \cos\gamma_k \cos\theta_k^{(\ell,h)} \sin\phi_k^{(\ell,h)} \\ \cos\gamma_k \sin\theta_k^{(\ell,h)} \end{bmatrix} \\ &= |c_k|\, g_h^{(\ell)} \begin{bmatrix} -\sin\gamma_k \sin\phi_k^{(\ell,h)} \cos\eta_k - \cos\gamma_k \cos\theta_k^{(\ell,h)} \cos\phi_k^{(\ell,h)} \\ \sin\gamma_k \cos\phi_k^{(\ell,h)} \cos\eta_k - \cos\gamma_k \cos\theta_k^{(\ell,h)} \sin\phi_k^{(\ell,h)} \\ \cos\gamma_k \sin\theta_k^{(\ell,h)} \end{bmatrix} \\ &\quad + j\,|c_k|\, g_h^{(\ell)} \begin{bmatrix} -\sin\gamma_k \sin\phi_k^{(\ell,h)} \sin\eta_k \\ \sin\gamma_k \cos\phi_k^{(\ell,h)} \sin\eta_k \\ 0 \end{bmatrix}. \end{aligned} \tag{21}$$

The kth source's azimuth arrival angle $\phi_k^{(\ell,e)}$ has a support range of $[-\pi, \pi)$, which may be segmented into three disjoint subranges:

1.
$$\phi_k^{(\ell,h)} \in \left[-\frac{\pi}{2}, -\frac{\pi}{2}\right] \Leftrightarrow \cos\phi_k^{(\ell,h)} > 0 \;\Leftrightarrow\; \widehat{\mathrm{sgn}}\left\{\sin(\eta_k)\right\} \Im\left\{\left[\hat{\mathbf{a}}_k^{(\ell)} e^{-j\angle\left[\hat{\mathbf{a}}_k^{(\ell)}\right]_6}\right]_5\right\} > 0,$$

2.
$$\begin{aligned} \phi_k^{(\ell,h)} \in \left(\frac{\pi}{2}, \pi\right] \Leftrightarrow \cos\phi_k^{(\ell,h)} < 0 \;\text{ and }\; \sin\phi_k^{(\ell,h)} > 0 \Leftrightarrow \widehat{\mathrm{sgn}}\left\{\sin(\eta_k)\right\} \Im\left\{\left[\hat{\mathbf{a}}_k^{(\ell)} e^{-j\angle\left[\hat{\mathbf{a}}_k^{(\ell)}\right]_6}\right]_5\right\} \\ < 0,\ \widehat{\mathrm{sgn}}\left\{\sin(\eta_k)\right\} \Im\left\{\left[\hat{\mathbf{a}}_k^{(\ell)} e^{-j\angle\left[\hat{\mathbf{a}}_k^{(\ell)}\right]_6}\right]_4\right\} < 0, \end{aligned}$$

3.
$$\begin{aligned} \phi_k^{(\ell,h)} \in \left[-\pi, -\frac{\pi}{2}\right) \Leftrightarrow \cos\phi_k^{(\ell,h)} < 0 \;\text{ and }\; \sin\phi_k^{(\ell,h)} < 0 \Leftrightarrow \widehat{\mathrm{sgn}}\left\{\sin(\eta_k)\right\} \Im\left\{\left[\hat{\mathbf{a}}_k^{(\ell)} e^{-j\angle\left[\hat{\mathbf{a}}_k^{(\ell)}\right]_6}\right]_5\right\} \\ < 0,\ \widehat{\mathrm{sgn}}\left\{\sin(\eta_k)\right\} \Im\left\{\left[\hat{\mathbf{a}}_k^{(\ell)} e^{-j\angle\left[\hat{\mathbf{a}}_k^{(\ell)}\right]_6}\right]_4\right\} > 0. \end{aligned}$$

Then, straightforward manipulations of (15) yield (22) (please see equation (61) in *He and Liu* [2009], Composition 1.2 in Table 1 of *Yuan et al.* [2012]). Some similar but mistaken expression appears in equation (9) of *Wong* [2001].

The elevation arrival angle $\theta_k^{(\ell,e)}$ has a support range of $[0, \pi]$, which may be segmented into two disjoint subranges:

1.
$$\begin{aligned} \theta_k^{(\ell,h)} \in \left[0, \frac{\pi}{2}\right) \;\Leftrightarrow\; \cos\theta_k^{(\ell,h)} > 0 \Leftrightarrow \Re\left\{\left[\hat{\mathbf{a}}_k^{(\ell)}\right]_4 e^{-j\angle\left[\hat{\mathbf{a}}_k^{(\ell)}\right]_6}\right\} \cos\hat{\phi}_k^{(\ell,h)} \\ + \Re\left\{\left[\hat{\mathbf{a}}_k^{(\ell)}\right]_5 e^{-j\angle\left[\hat{\mathbf{a}}_k^{(\ell)}\right]_6}\right\} \sin\hat{\phi}_k^{(\ell,h)} < 0, \end{aligned}$$

2.

$$\theta_k^{(\ell,h)} \in \left[\frac{\pi}{2}, \pi\right] \Leftrightarrow \cos\theta_k^{(\ell,h)} < 0 \Leftrightarrow \Re\left\{\left[\hat{\mathbf{a}}_k^{(\ell)}\right]_4 e^{-j\angle\left[\hat{\mathbf{a}}_k^{(\ell)}\right]_6}\right\}\cos\hat{\phi}_k^{(\ell,h)} + \Re\left\{\left[\hat{\mathbf{a}}_k^{(\ell)}\right]_5 e^{-j\angle\left[\hat{\mathbf{a}}_k^{(\ell)}\right]_6}\right\}\sin\hat{\phi}_k^{(\ell,h)} > 0.$$

Then, straightforward manipulations of (15) yield (23) (please see equation (62) in *He and Liu* [2009], Composition 1.2 in Table 1 of *Yuan et al.* [2012]). Some similar but mistaken expression appears in equation (10) of *Wong* [2001].

$$\hat{\phi}_k^{(\ell,h)} = \begin{cases} \arctan\left(-\dfrac{\Im\left\{\left[\hat{\mathbf{a}}_k^{(\ell)} e^{-j\angle\left[\hat{\mathbf{a}}_k^{(\ell)}\right]_6}\right]_4\right\}}{\Im\left\{\left[\hat{\mathbf{a}}_k^{(\ell)} e^{-j\angle\left[\hat{\mathbf{a}}_k^{(\ell)}\right]_6}\right]_5\right\}}\right), & \text{if } \widehat{\operatorname{sgn}}\left\{\sin(\eta_k)\right\}\Im\left\{\left[\hat{\mathbf{a}}_k^{(\ell)} e^{-j\angle\left[\hat{\mathbf{a}}_k^{(\ell)}\right]_6}\right]_5\right\} > 0, \\ \pi + \arctan\left(-\dfrac{\Im\left\{\left[\hat{\mathbf{a}}_k^{(\ell)} e^{-j\angle\left[\hat{\mathbf{a}}_k^{(\ell)}\right]_6}\right]_4\right\}}{\Im\left\{\left[\hat{\mathbf{a}}_k^{(\ell)} e^{-j\angle\left[\hat{\mathbf{a}}_k^{(\ell)}\right]_6}\right]_5\right\}}\right), & \text{if } \begin{array}{l}\widehat{\operatorname{sgn}}\left\{\sin(\eta_k)\right\}\Im\left\{\left[\hat{\mathbf{a}}_k^{(\ell)} e^{-j\angle\left[\hat{\mathbf{a}}_k^{(\ell)}\right]_6}\right]_5\right\} < 0, \text{ and} \\ \widehat{\operatorname{sgn}}\left\{\sin(\eta_k)\right\}\Im\left\{\left[\hat{\mathbf{a}}_k^{(\ell)} e^{-j\angle\left[\hat{\mathbf{a}}_k^{(\ell)}\right]_6}\right]_4\right\} < 0\end{array} \\ -\pi + \arctan\left(-\dfrac{\Im\left\{\left[\hat{\mathbf{a}}_k^{(\ell)} e^{-j\angle\left[\hat{\mathbf{a}}_k^{(\ell)}\right]_6}\right]_4\right\}}{\Im\left\{\left[\hat{\mathbf{a}}_k^{(\ell)} e^{-j\angle\left[\hat{\mathbf{a}}_k^{(\ell)}\right]_6}\right]_5\right\}}\right), & \text{if } \begin{array}{l}\widehat{\operatorname{sgn}}\left\{\sin(\eta_k)\right\}\Im\left\{\left[\hat{\mathbf{a}}_k^{(\ell)} e^{-j\angle\left[\hat{\mathbf{a}}_k^{(\ell)}\right]_6}\right]_5\right\} < 0, \text{ and} \\ \widehat{\operatorname{sgn}}\left\{\sin(\eta_k)\right\}\Im\left\{\left[\hat{\mathbf{a}}_k^{(\ell)} e^{-j\angle\left[\hat{\mathbf{a}}_k^{(\ell)}\right]_6}\right]_4\right\} > 0\end{array} \end{cases} \tag{22}$$

$$\hat{\theta}_k^{(\ell,h)} = \begin{cases} \arctan\left\{\left|\dfrac{\left[\hat{\mathbf{a}}_k^{(\ell)}\right]_6}{\Re\left\{\left[\hat{\mathbf{a}}_k^{(\ell)}\right]_4 e^{-j\angle\left[\hat{\mathbf{a}}_k^{(\ell)}\right]_6}\right\}\cos\hat{\phi}_k^{(\ell,h)} + \Re\left\{\left[\hat{\mathbf{a}}_k^{(\ell)}\right]_5 e^{-j\angle\left[\hat{\mathbf{a}}_k^{(\ell)}\right]_6}\right\}\sin\hat{\phi}_k^{(\ell,h)}}\right|\right\}, \\ \text{if } \Re\left\{\left[\hat{\mathbf{a}}_k^{(\ell)}\right]_4 e^{-j\angle\left[\hat{\mathbf{a}}_k^{(\ell)}\right]_6}\right\}\cos\hat{\phi}_k^{(\ell,h)} + \Re\left\{\left[\hat{\mathbf{a}}_k^{(\ell)}\right]_5 e^{-j\angle\left[\hat{\mathbf{a}}_k^{(\ell)}\right]_6}\right\}\sin\hat{\phi}_k^{(\ell,h)} < 0, \\ \pi + \arctan\left\{\left|\dfrac{\left[\hat{\mathbf{a}}_k^{(\ell)}\right]_6}{\Re\left\{\left[\hat{\mathbf{a}}_k^{(\ell)}\right]_5 e^{-j\angle\left[\hat{\mathbf{a}}_k^{(\ell)}\right]_6}\right\}\cos\hat{\phi}_k^{(\ell,h)} + \Re\left\{\left[\hat{\mathbf{a}}_k^{(\ell)}\right]_4 e^{-j\angle\left[\hat{\mathbf{a}}_k^{(\ell)}\right]_6}\right\}\sin\hat{\phi}_k^{(\ell,h)}}\right|\right\}, \\ \text{if } \Re\left\{\left[\hat{\mathbf{a}}_k^{(\ell)}\right]_4 e^{-j\angle\left[\hat{\mathbf{a}}_k^{(\ell)}\right]_6}\right\}\cos\hat{\phi}_k^{(\ell,h)} + \Re\left\{\left[\hat{\mathbf{a}}_k^{(\ell)}\right]_5 e^{-j\angle\left[\hat{\mathbf{a}}_k^{(\ell)}\right]_6}\right\}\sin\hat{\phi}_k^{(\ell,h)} > 0. \end{cases} \tag{23}$$

Based on equations (11) and (12) in *Wong* [2001], equations (63) and (64) in *He and Liu* [2009], or Composition 1.2 in Table 1 in *Yuan et al.* [2012],

$$\hat{\gamma}_k^{(\ell,h)} = \arccos\left|\frac{1}{\hat{g}_h^{(\ell)}}\frac{\left[\hat{\mathbf{a}}_k^{(\ell)}\right]_6/|c_k|}{\sin\hat{\theta}_k^{(\ell,h)}}\right|, \tag{24}$$

$$\hat{\eta}_k^{(\ell,h)} = -\angle\left(\left[\hat{\mathbf{a}}_k^{(\ell)} e^{-j\angle\left[\hat{\mathbf{a}}_k^{(\ell)}\right]_6}\right]_5\cos\hat{\phi}_k^{(\ell,h)} - \left[\hat{\mathbf{a}}_k^{(\ell)} e^{-j\angle\left[\hat{\mathbf{a}}_k^{(\ell)}\right]_6}\right]_4\sin\hat{\phi}_k^{(\ell,h)}\right). \tag{25}$$

As in section 6.2 for the dipole triads, the above estimation for $\{\hat{\theta}_k^{(\ell,h)}, \hat{\phi}_k^{(\ell,h)}, \hat{\eta}_k^{(\ell,h)}\}$ in (23)–(25) is *in*dependent of the gain uncertainties of the loop triads and is independent of the a priori unknown complex-value scalar c_k.

6.4. Considering the Entire Array of *L* Electromagnetic Vector Sensors

As one of these two triads (either the dipole triad or the magnetic triad in the $\ell = 1$st electromagnetic vector sensor) serves as orientational reference for all *L* electromagnetic vector sensors, the *k*th incident source's

azimuth angle, elevation angle, and polarization parameters, respectively, may be estimated as

$$\hat{\theta}_k = \begin{cases} \hat{\theta}_k^{(1,e)}, & \text{if the } \ell = 1\text{st dipole triad is orient. ref.} \\ \hat{\theta}_k^{(1,h)}, & \text{if the } \ell = 1\text{st loop triad is orient. ref.} \end{cases} \tag{26}$$

$$\hat{\phi}_k = \begin{cases} \hat{\phi}_k^{(1,e)}, & \text{if the } \ell = 1\text{st dipole triad is orient. ref.,} \\ \hat{\phi}_k^{(1,h)}, & \text{if the } \ell = 1\text{st loop triad is orient. ref.,} \end{cases} \tag{27}$$

$$\hat{\gamma}_k = \frac{1}{2L}\left(\sum_{\ell=1}^{L} \hat{\gamma}_k^{(\ell,e)} + \sum_{\ell=1}^{L} \hat{\gamma}_k^{(\ell,h)}\right), \tag{28}$$

$$\hat{\eta}_k = \frac{1}{2L}\left(\sum_{\ell=1}^{L} \hat{\eta}_k^{(\ell,e)} + \sum_{\ell=1}^{L} \hat{\eta}_k^{(\ell,h)}\right). \tag{29}$$

In the above (26) to (29), averaging over ℓ (i.e., averaging over the L electromagnetic vector sensors) is performed only for the polarization estimates but not for the direction-of-arrival estimates. This is because only the latter is unaffected by any misorientation in the nonreference vector sensors; and misorientation calibration will be performed next in section 7.

7. Proposed Algorithm's Step #4: "Blind" Calibration of Each Vector Sensor's Misorientation

This section will develop the misorientation calibration algorithm for Step #4. Step #4 here may be executed in parallel with Step #5 in section 8 for phase uncertainty calibration, and/or simultaneously with Step #6 in section 9 for mislocation calibration.

For the kth source measured by the ℓth (possibly) misoriented dipole triad/loop triad,

$$\begin{bmatrix} u_k^{(\ell,\varsigma)} \\ v_k^{(\ell,\varsigma)} \\ w_k^{(\ell,\varsigma)} \end{bmatrix} = \mathbf{R}\left(\alpha^{(\ell,\varsigma)}, \varphi^{(\ell,\varsigma)}, \psi^{(\ell,\varsigma)}\right) \begin{bmatrix} u_k \\ v_k \\ w_k \end{bmatrix}, \quad \forall k, \ell, \varsigma,$$

where $\varsigma = e$ for a dipole triad but $\varsigma = h$ for a loop triad. The 3×3 matrix $\mathbf{R}\left(\theta^{(\ell,\varsigma)}, \gamma^{(\ell,\varsigma)}, \phi^{(\ell,\varsigma)}\right)$ has been defined in (5).

Considering all K sources under noisy conditions, $\forall \ell = 2, 3, \ldots, L$,

$$\underbrace{\begin{bmatrix} \hat{u}_1 & \hat{v}_1 & \hat{w}_1 \\ \vdots & \vdots & \vdots \\ \hat{u}_K & \hat{v}_K & \hat{w}_K \end{bmatrix}}_{\stackrel{\text{def}}{=}\boldsymbol{\Gamma}} \left[\mathbf{R}\left(\alpha^{(\ell,\varsigma)}, \varphi^{(\ell,\varsigma)}, \psi^{(\ell,\varsigma)}\right)\right]^T \approx \underbrace{\begin{bmatrix} \hat{u}_1^{(\ell,\varsigma)} & \hat{v}_1^{(\ell,\varsigma)} & \hat{w}_1^{(\ell,\varsigma)} \\ \vdots & \vdots & \vdots \\ \hat{u}_K^{(\ell,\varsigma)} & \hat{v}_K^{(\ell,\varsigma)} & \hat{w}_K^{(\ell,\varsigma)} \end{bmatrix}}_{\stackrel{\text{def}}{=}\boldsymbol{\Gamma}^{(\ell,\varsigma)}}, \tag{30}$$

where

$$\begin{bmatrix} \hat{u}_k \\ \hat{v}_k \\ \hat{w}_k \end{bmatrix} = \begin{bmatrix} \sin\hat{\theta}_k \cos\hat{\phi}_k \\ \sin\hat{\theta}_k \sin\hat{\phi}_k \\ \cos\hat{\theta}_k \end{bmatrix}, \tag{31}$$

$$\begin{bmatrix} \hat{u}_k^{(\ell,\varsigma)} \\ \hat{v}_k^{(\ell,\varsigma)} \\ \hat{w}_k^{(\ell,\varsigma)} \end{bmatrix} = \begin{bmatrix} \sin\hat{\theta}_k^{(\ell,\varsigma)} \cos\hat{\phi}_k^{(\ell,\varsigma)} \\ \sin\hat{\theta}_k^{(\ell,\varsigma)} \sin\hat{\phi}_k^{(\ell,\varsigma)} \\ \cos\hat{\theta}_k^{(\ell,\varsigma)} \end{bmatrix}. \tag{32}$$

The above $K \times 3$ matrix $\boldsymbol{\Gamma}$, defined in an underbrace in (30), contains all K sources' direction cosines measured from the $\ell = 1$st dipole triad/loop triad, which serves as orientational reference. Similarly, the $K \times 3$ matrix $\boldsymbol{\Gamma}^{(\ell,\varsigma)}$, also defined in an underbrace in (30), contains all K sources' direction cosines measured from the $\ell \neq 1$st misoriented dipole triad/loop triad. Moreover, in (31), $\hat{\theta}_k$ has been computed in (26), and $\hat{\phi}_k$ computed in (27). Likewise in (32), $\hat{\theta}_k^{(\ell,\varsigma)}$ has been evaluated in (17) or (23), and $\hat{\phi}_k^{(\ell,\varsigma)}$ computed in (16) or (22).

Therefore, the misorientation matrix $\mathbf{R}\left(\alpha^{(\ell,\varsigma)}, \varphi^{(\ell,\varsigma)}, \psi^{(\ell,\varsigma)}\right)$ may be estimated as

$$\hat{\mathbf{R}}^{(\ell,\varsigma)} = \left[\left(\mathbf{\Gamma}^H\mathbf{\Gamma}\right)^{-1}\mathbf{\Gamma}^H\mathbf{\Gamma}^{(\ell,\varsigma)}\right]^T. \tag{33}$$

The above $\hat{\mathbf{R}}^{(\ell,\varsigma)}$ would be full ranked for any $K \geq 3$, except at a few particular parametric values that could occur with only zero probability, due to the noises in the data model. Specifically at $K = 3$, the simplification of $\left(\mathbf{\Gamma}^H\mathbf{\Gamma}\right)^{-1}\mathbf{\Gamma}^H = \mathbf{\Gamma}^{-1}$ holds.

The misorientation matrix $\mathbf{R}\left(\alpha^{(\ell,\varsigma)}, \varphi^{(\ell,\varsigma)}, \psi^{(\ell,\varsigma)}\right)$ in (5) may be rewritten as

$$\begin{aligned}
\left[\mathbf{R}\left(\alpha^{(\ell,\varsigma)}, \varphi^{(\ell,\varsigma)}, \psi^{(\ell,\varsigma)}\right)\right]_{1,2} &= \cos\varphi^{(\ell,\varsigma)}\sin\psi^{(\ell,\varsigma)},\\
\left[\mathbf{R}\left(\alpha^{(\ell,\varsigma)}, \varphi^{(\ell,\varsigma)}, \psi^{(\ell,\varsigma)}\right)\right]_{2,2} &= \cos\varphi^{(\ell,\varsigma)}\cos\psi^{(\ell,\varsigma)},\\
\left[\mathbf{R}\left(\alpha^{(\ell,\varsigma)}, \varphi^{(\ell,\varsigma)}, \psi^{(\ell,\varsigma)}\right)\right]_{3,1} &= -\cos\varphi^{(\ell,\varsigma)}\sin\alpha^{(\ell,\varsigma)},\\
\left[\mathbf{R}\left(\alpha^{(\ell,\varsigma)}, \varphi^{(\ell,\varsigma)}, \psi^{(\ell,\varsigma)}\right)\right]_{3,2} &= -\sin\varphi^{(\ell,\varsigma)},\\
\left[\mathbf{R}\left(\alpha^{(\ell,\varsigma)}, \varphi^{(\ell,\varsigma)}, \psi^{(\ell,\varsigma)}\right)\right]_{3,3} &= \cos\varphi^{(\ell,\varsigma)}\cos\alpha^{(\ell,\varsigma)},
\end{aligned}$$

where $[\cdot]_{i,j}$ denotes the (i,j)th entry of the matrix inside the square brackets. For explicit estimation of the ℓth dipole triad's/loop triad's misorientation parameters, $\forall \ell = 2, 3, \ldots, L$,

$$\hat{\alpha}^{(\ell,\varsigma)} = -\arctan\left(\frac{\left[\hat{\mathbf{R}}^{(\ell,\varsigma)}\right]_{3,1}}{\left[\hat{\mathbf{R}}^{(\ell,\varsigma)}\right]_{3,3}}\right), \tag{34}$$

$$\hat{\varphi}^{(\ell,\varsigma)} = -\arcsin\left(\left[\hat{\mathbf{R}}^{(\ell,\varsigma)}\right]_{3,2}\right), \tag{35}$$

$$\hat{\psi}^{(\ell,\varsigma)} = \arctan\left(\frac{\left[\hat{\mathbf{R}}^{(\ell,\varsigma)}\right]_{1,2}}{\left[\hat{\mathbf{R}}^{(\ell,\varsigma)}\right]_{2,2}}\right). \tag{36}$$

The present work, to the best of the present authors' knowledge, is first in the open literature to "blindly" calibrate an electromagnetic vector sensor of arbitrary misorientation. The algorithms in *Jia-cai et al.* [2009a, 2009b] and *You et al.* [2010] are invalid, because they fundamentally misunderstand how misorientation would affect the electromagnetic vector sensor. Please refer to section 1.2.

8. Proposed Algorithm's Step #5: Calibration of the Vector Sensors' Phase Uncertainty

From the phase uncertainty model in (4), the ℓth vector sensor would have either $\epsilon_e^{(\ell)}$ or $\epsilon_h^{(\ell)}$ serving as a phase reference and thus prior known.

From (2), the kth source's ℓth electromagnetic vector sensor steering vector may be expressed as

$$\begin{aligned}
\hat{\mathbf{a}}_k^{(\ell)} \approx c_k\, e^{j\frac{2\pi f_k}{c}\left\{\left(x^{(\ell)}+\Delta_x^{(\ell)}\right)u_k+\left(y^{(\ell)}+\Delta_y^{(\ell)}\right)v_k+\left(z^{(\ell)}+\Delta_z^{(\ell)}\right)w_k\right\}}\\
\cdot\begin{bmatrix}
g_e^{(\ell)}\, e^{j\epsilon_e^{(\ell)}}\left(\sin\gamma_k\cos\theta_k^{(\ell,e)}\cos\phi_k^{(\ell,e)}e^{j\eta_k}-\cos\gamma_k\sin\phi_k^{(\ell,e)}\right)\\
g_e^{(\ell)}\, e^{j\epsilon_e^{(\ell)}}\left(\sin\gamma_k\cos\theta_k^{(\ell,e)}\sin\phi_k^{(\ell,e)}e^{j\eta_k}+\cos\gamma_k\cos\phi_k^{(\ell,e)}\right)\\
g_e^{(\ell)}\, e^{j\epsilon_e^{(\ell)}}\left(-\sin\gamma_k\sin\theta_k^{(\ell,e)}e^{j\eta_k}\right)\\
g_h^{(\ell)}\, e^{j\epsilon_h^{(\ell)}}\left(-\sin\gamma_k\sin\phi_k^{(\ell,h)}e^{j\eta_k}-\cos\gamma_k\cos\theta_k^{(\ell,h)}\cos\phi_k^{(\ell,h)}\right)\\
g_h^{(\ell)}\, e^{j\epsilon_h^{(\ell)}}\left(\sin\gamma_k\cos\phi_k^{(\ell,h)}e^{j\eta_k}-\cos\gamma_k\cos\theta_k^{(\ell,h)}\sin\phi_k^{(\ell,h)}\right)\\
g_h^{(\ell)}\, e^{j\epsilon_h^{(\ell)}}\left(\cos\gamma_k\sin\theta_k^{(\ell,h)}\right)
\end{bmatrix}.
\end{aligned} \tag{37}$$

Hence, the phase difference between the ℓth dipole triad and the ℓth loop triad equals $e^{j(\epsilon_h^{(\ell)}-\epsilon_e^{(\ell)})} \approx -\frac{\left[\hat{\mathbf{a}}_k^{(\ell)}\right]_6}{\left[\hat{\mathbf{a}}_k^{(\ell)}\right]_3} e^{j\eta_k}$.

If $\epsilon_e^{(\ell)}$ serves as a phase reference for the ℓth electromagnetic vector sensor, (see equation (16) in *Lan-mei et al.* [2007])

$$\hat{\epsilon}_h^{(\ell)} = \angle\left(-\frac{\left[\hat{\mathbf{a}}_k^{(\ell)}\right]_6}{\left[\hat{\mathbf{a}}_k^{(\ell)}\right]_3}\right) + \epsilon_e^{(\ell)} + \hat{\eta}_k, \tag{38}$$

where $\hat{\eta}_k$ has been estimated in (29).

Similarly, if $\epsilon_h^{(\ell)}$ serves as a phase reference for the ℓth electromagnetic vector sensor, (see equation (16) in *Lan-mei et al.* [2007])

$$\hat{\epsilon}_e^{(\ell)} = \angle\left(-\frac{\left[\hat{\mathbf{a}}_k^{(\ell)}\right]_3}{\left[\hat{\mathbf{a}}_k^{(\ell)}\right]_6}\right) + \epsilon_h^{(\ell)} - \hat{\eta}_k. \tag{39}$$

The above step is viable for any $K \geq 1$. This step requires only the prior estimation of η_k but is algorithmically independent from the calibration of misorientation in section 7 and the calibration of mislocation in section 9.

9. Proposed Algorithm's Step #6: Calibration of the Vector Sensors' Mislocation

Recall the dislocation modeling under point (5) in section 2. The ℓth ($\ell \geq 2$) vector sensor's spatial phase factor equals

$$\beta_k^{(\ell)} \overset{\text{def}}{=} \begin{cases} \angle\left(\left[\hat{\mathbf{a}}_k^{(\ell)}\right]_3 / \left[\hat{\mathbf{a}}_k^{(1)}\right]_3 / q_k^{(\ell)}\right) - \epsilon_e^{(\ell)} + \epsilon_e^{(1)}, & \text{if } \epsilon_e^{(1)} \text{ and } \epsilon_e^{(\ell)} \text{ are prior known;} \\ \angle\left(-\left[\hat{\mathbf{a}}_k^{(\ell)}\right]_6 / \left[\hat{\mathbf{a}}_k^{(1)}\right]_3 / q_k^{(\ell)}\right) - \epsilon_h^{(\ell)} + \epsilon_e^{(1)} + \hat{\eta}_k, & \text{if } \epsilon_e^{(1)} \text{ and } \epsilon_h^{(\ell)} \text{are prior known;} \\ \angle\left(-\left[\hat{\mathbf{a}}_k^{(\ell)}\right]_3 / \left[\hat{\mathbf{a}}_k^{(1)}\right]_6 / q_k^{(\ell)}\right) - \epsilon_e^{(\ell)} + \epsilon_h^{(1)} - \hat{\eta}_k, & \text{if } \epsilon_h^{(1)} \text{ and } \epsilon_e^{(\ell)} \text{are prior known;} \\ \angle\left(\left[\hat{\mathbf{a}}_k^{(\ell)}\right]_6 / \left[\hat{\mathbf{a}}_k^{(1)}\right]_6 / q_k^{(\ell)}\right) - \epsilon_h^{(\ell)} + \epsilon_h^{(1)}, & \text{if } \epsilon_h^{(1)} \text{ and } \epsilon_h^{(\ell)} \text{ are prior known.} \end{cases} \tag{40}$$

Accounting for all $K \geq 3$ sources,

$$\underbrace{\begin{bmatrix} \frac{2\pi}{\hat{\lambda}_1}\hat{u}_1 & \frac{2\pi}{\hat{\lambda}_1}\hat{v}_1 & \frac{2\pi}{\hat{\lambda}_1}\hat{w}_1 \\ \vdots & \vdots & \vdots \\ \frac{2\pi}{\hat{\lambda}_K}\hat{u}_K & \frac{2\pi}{\hat{\lambda}_K}\hat{v}_K & \frac{2\pi}{\hat{\lambda}_K}\hat{w}_K \end{bmatrix}}_{\overset{\text{def}}{=}\mathbf{\Pi}} \underbrace{\begin{bmatrix} \Delta_x^{(\ell)} \\ \Delta_y^{(\ell)} \\ \Delta_z^{(\ell)} \end{bmatrix}}_{\overset{\text{def}}{=}\boldsymbol{\epsilon}} \approx \underbrace{\begin{bmatrix} \beta_1^{(\ell)} \\ \vdots \\ \beta_K^{(\ell)} \end{bmatrix}}_{\overset{\text{def}}{=}\boldsymbol{\nu}}.$$

where $\varsigma = e$ if the dipole triad serves as reference, but $\varsigma = h$ if the loop triad is the designated reference. Furthermore, $\hat{\lambda}_k = \frac{2\pi c \triangle_T}{\angle[\mathbf{\Phi}]_{k,k}}$, where c symbolizes the speed of light and $\mathbf{\Phi}$ has been defined inside {3} in section 4.

The dislocation is assumed here as sufficiently small, such that no 2π cyclic ambiguity arises; i.e., the dislocation would be a fraction of a wavelength. Hence, $\{\Delta_x^{(\ell)}, \Delta_y^{(\ell)}, \Delta_z^{(\ell)}\}$ may be estimated as

$$\hat{\Delta}_x^{(\ell)} = [\boldsymbol{\epsilon}]_1, \tag{41}$$

$$\hat{\Delta}_y^{(\ell)} = [\boldsymbol{\epsilon}]_2, \tag{42}$$

$$\hat{\Delta}_z^{(\ell)} = [\boldsymbol{\epsilon}]_3, \tag{43}$$

where

$$\boldsymbol{\epsilon} \overset{\text{def}}{=} \left[\left(\mathbf{\Pi}^H\mathbf{\Pi}\right)^{-1}\mathbf{\Pi}^H\boldsymbol{\nu}\right]^T. \tag{44}$$

Table 1. The Five Nonideal Electromagnetic Vector Sensors' Actual Cartesian Locations, Actual Mislocations, Actual Misorientations, and Actual Gain Nonidealities

ℓ	1	2	3	4	5
$\frac{(x_\ell, y_\ell, z_\ell)}{\lambda_{\min}}$	(0, 0, 0)	(0.1, 0.1, 0)	(0.15, 0.15, 0)	(0.2, 0.2, 0)	(0.25, 0.25, 0)
$\frac{(\Delta_x^{(\ell)}, \Delta_y^{(\ell)}, \Delta_z^{(\ell)})}{\lambda_{\min}}$	(0, 0, 0)	(0.01, 0.02, 0.012)	(0.011, 0.018, 0.017)	(0.015, 0.008, 0.006)	(0.002, 0.016, 0.010)
$(\alpha^{(\ell,e)}, \varphi^{(\ell,e)}, \psi^{(\ell,e)})$	(0°, 0°, 0°)	(8°, 5°, 3°)	(6°, 2°, 7°)	(3°, 5°, 7°)	(9°, 6°, 5°)
$(\alpha^{(\ell,h)}, \varphi^{(\ell,h)}, \psi^{(\ell,h)})$	(8°, 2°, 5°)	(6°, 7°, 4°)	(6°, 4°, 2°)	(8°, 3°, 6°)	(9°, 5°, 8°)
$(g_e^{(\ell)}, g_h^{(\ell)})$	(1.00, 1.20)	(1.11, 1.50)	(1.43, 1.30)	(0.80, 0.65)	(1.95, 0.86)
$\frac{(\epsilon_e^{(\ell)}, \epsilon_h^{(\ell)})}{\pi}$	(0.8593, −0.6075)	(−0.5261, −0.7904)	(−0.2242, −0.2870)	(−0.4271, 0.3162)	(−0.6999, −0.0052)

The above $\mathbf{\Pi}$ would be full ranked for any $K \geq 3$, except at a few particular sets of parametric values that occur with zero probability due to the noises in the data model. Hence, this step is viable for any $K \geq 3$. Specifically at $K = 3$, the simplification of $\left(\mathbf{\Pi}^H \mathbf{\Pi}\right)^{-1} \mathbf{\Pi}^H = \mathbf{\Pi}^{-1}$ holds.

Incidentally, this step requires the prior estimation of only η_k but is algorithmically independent of the calibration of the misorientation in section 7 and the calibration of the phase uncertainties in section 8.

10. Monte Carlo Simulations

10.1. The Proposed Scheme's Efficacy for "Blind" Calibration and Direction Finding

This section presents Monte Carlo simulations to verify the efficacy of the proposed scheme developed in sections 4 to 9.

The simulation scenario is detailed below: There exist $K = 3$ pure tone incident signals, at digital frequencies (i.e., cycles per time sample), $f_1' = 0.14$, $f_2' = 0.23$, and $f_3' = 0.31$, which are a priori unknown to the receiver. Each pure tone has a random phase, uniformly distributed between $[0, 2\pi)$ radians, independently generated at each Monte Carlo trial, and statistically independent across the signals. Their respective emitters' azimuth-elevation directions-of-arrival and polarization parameters are $(\theta_1, \phi_1, \gamma_1, \eta_1) = (70°, 10°, 45°, 30°)$, $(\theta_2, \phi_2, \gamma_2, \eta_2) = (30°, -55°, 45°, 45°)$, and $(\theta_3, \phi_3, \gamma_3, \eta_3) = (60°, 100°, 60°, 60°)$, all of which are a priori unknown to the receiver. There exist $L = 5$ nonideal electromagnetic vector sensors, with nonideal gains, misorientations, and mislocations as indicated in Table 1. Referring to the phase uncertainty model in (4), Figures 2 and 3 have phase references $\epsilon_e^{(1)}, \epsilon_h^{(2)}, \epsilon_e^{(3)}, \epsilon_e^{(4)}$, and $\epsilon_h^{(5)}$. Each Monte Carlo trial consists of $N = 400$ snapshots of data, each corrupted by additive Gaussian noise, which is statistically uncorrelated over time and across all dipoles/loops. Each figure's every icon consists of $I = 100$ statistically independent Monte Carlo trials.

The performance metrics are defined in Table 2. There on the "phase uncertainty" row, $\kappa^{(\ell)} \in \{0, 1\}$ serves as a flag to indicate if the entity to which it is multiplied is prior known. Moreover, $\delta_{\theta,k,i}$ ($\delta_{\phi,k,i}$) symbolizes the ith Monte Carlo trial's estimation error for θ_k (ϕ_k); $\mathrm{CRB}(g_\varsigma^{(1)}) = 0$ by definition; $\delta_{g_\varsigma^{(1)},i} = 0, \forall i$ also by definition where $\varsigma = e$ if $g_e^{(1)}$ is prior known, $\varsigma = h$ if $g_h^{(1)}$ is prior known; $\mathrm{CRB}(\alpha^{(1,e)}) + \mathrm{CRB}(\varphi^{(1,e)}) + \mathrm{CRB}(\psi^{(1,e)}) = 0$ by definition; $\delta^2_{\alpha^{(1,e)},i} + \delta^2_{\varphi^{(1,e)},i} + \delta^2_{\psi^{(1,e)},i} = 0, \forall i$ also by definition; and $\lambda_{\min}$ is defined as the minimum of $\lambda_1, \ldots, \lambda_K$.

The Monte Carlo simulations in Figure 2 verify that the proposed "blind" algorithm offers effective calibration. All angles are plotted in degrees (not in radians) in all figures. Specifically, for any SNR $\geq$15 dB, the polarization parameters are estimated to an MSE within 0.1°, the directions-of-arrival and phase uncertainty to under 1°, the misorientation angles to within 2°, the gain coefficients are estimated to about 0.003%, and the dislocation to within $0.00003\lambda_{\min}$.

10.2. The Proposed Scheme's Orders-of-Magnitude Computational Simplicity Over the Maximum Likelihood Estimation

To highlight the computational efficiency of the proposed scheme, it will be compared here against the maximum likelihood estimation (MLE) of the non-ideality parameters, the directions-of-arrival, and the polarization parameters.

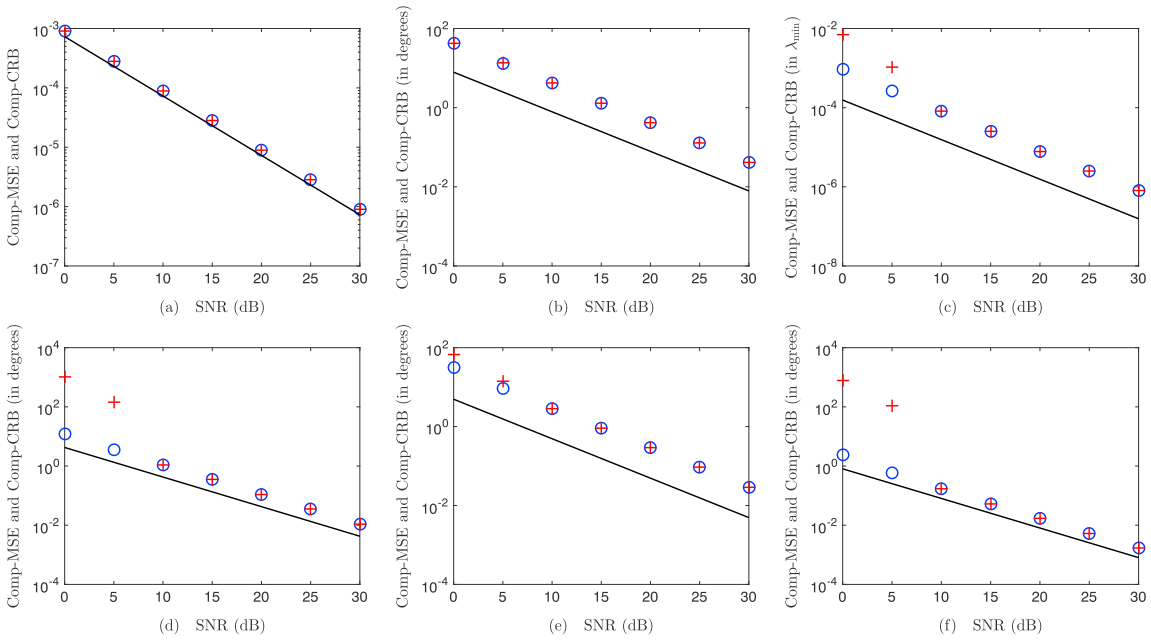

Figure 2. Monte Carlo simulations verify the efficacy of proposed scheme (in sections 4 to 9) for "blind" calibration of (a) intravector sensor gain uncertainties, (b) intertriad misorientations, (c) intertriad dislocations, and (d) intertriad phase uncertainties as well as for (e) direction finding and (f) polarization estimation, where the blue circle denotes proposed algorithm when $\mathrm{sgn}\{\sin(\eta_k)\}$ is prior known, while red cross denotes proposed algorithm when $\mathrm{sgn}\{\sin(\eta_k)\}$ is prior unknown, and the black solid line represents the composite CRB.

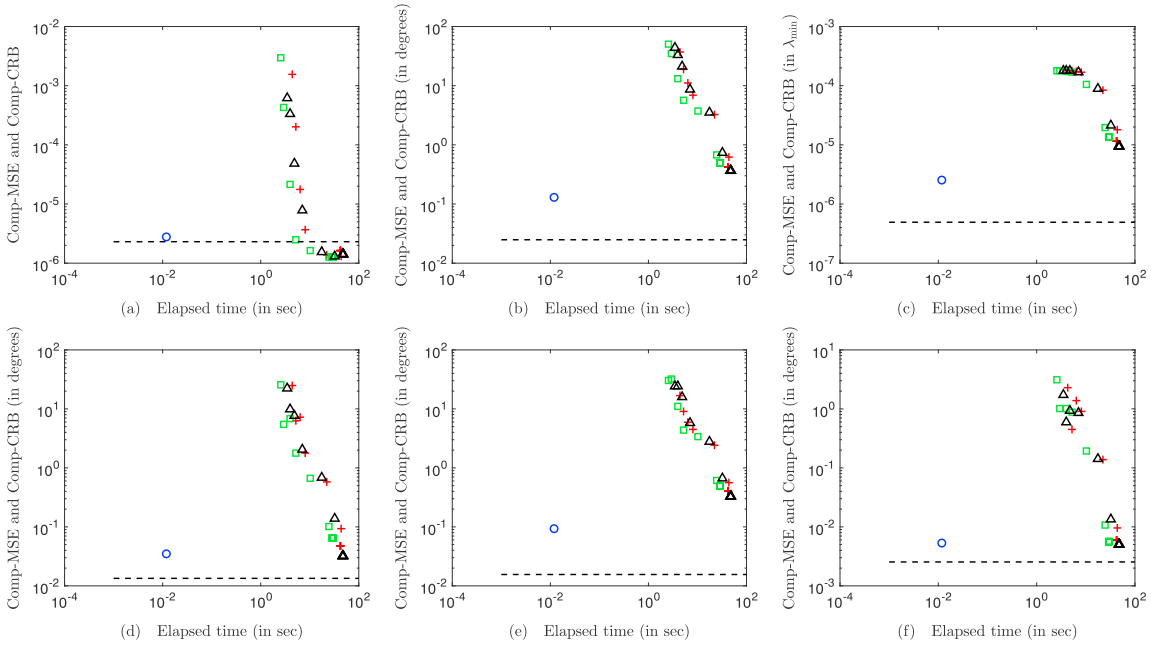

Figure 3. The proposed scheme (i.e., the lone circle icon at the lower left corner of each subfigure) requires only about 0.1% of the MLE's computational load, for comparable composite MSE's. Subfigures are the calibrations of (a) intravector sensor gain uncertainties, (b) intertriad misorientations, (c) intertriad dislocations, and (d) intertriad phase uncertainties as well as for (e) direction finding and (f) polarization estimation, where the blue circle denotes proposed algorithm, while red cross, green square, and black triangle denote, respectively, the MLE initialized at $(\theta_k + 5°, \phi_k + 5°, \gamma_k + 5°, \eta_k + 5°)$, $(\theta_k + 10°, \phi_k + 10°, \gamma_k + 10°, \eta_k + 10°)$, and $(\theta_k + 15°, \phi_k + 15°, \gamma_k + 15°, \eta_k + 15°)$, and the black dashed line represents the composite CRB.

Table 2. Definition of Performance Metrics Plotted in Figure 2

	Composite Mean-Square Error (Comp-MSE)	Composite Cramér-Rao Bound (Comp-CRB)
Directions-of-arrival	$\frac{1}{2KI}\sum_{k=1}^{K}\sum_{i=1}^{I}\left(\delta^2_{\theta,k,i}+\delta^2_{\phi,k,i}\right)$	$\frac{1}{2K}\sum_{k=1}^{K}\left(\mathrm{CRB}(\theta_k)+\mathrm{CRB}(\phi_k)\right)$
Polarization parameters	$\frac{1}{2KI}\sum_{k=1}^{K}\sum_{i=1}^{I}\left(\delta^2_{\gamma,k,i}+\delta^2_{\eta,k,i}\right)$	$\frac{1}{2K}\sum_{k=1}^{K}\left(\mathrm{CRB}(\gamma_k)+\mathrm{CRB}(\eta_k)\right)$
Gain uncertainty	$\frac{1}{2LI}\sum_{i=1}^{I}\sum_{\ell=1}^{L}\left(\delta^2_{g_e^{(\ell)},i}+\delta^2_{g_h^{(\ell)},i}\right)$	$\frac{1}{2L}\sum_{\ell=1}^{L}\left[\mathrm{CRB}(g_e^{(\ell)})+\mathrm{CRB}(g_h^{(\ell)})\right]$
Phase uncertainty	$\frac{1}{LI}\sum_{i=1}^{I}\sum_{\ell=1}^{L}\left(\kappa^{(\ell)}\delta^2_{\epsilon_e^{(\ell)},i}+\left(1-\kappa^{(\ell)}\right)\delta^2_{\epsilon_h^{(\ell)},i}\right)$	$\frac{1}{L}\sum_{\ell=1}^{L}\left[\kappa^{(\ell)}\mathrm{CRB}(\epsilon_e^{(\ell)})+(1-\kappa^{(\ell)})\mathrm{CRB}(\epsilon_h^{(\ell)})\right]$
Misorientation	$\frac{1}{6LI}\sum_{i=1}^{I}\sum_{\ell=1}^{L}\left(\delta^2_{\alpha^{(\ell,e)},i}+\delta^2_{\varphi^{(\ell,e)},i}+\delta^2_{\psi^{(\ell,e)},i}+\delta^2_{\alpha^{(\ell,h)},i}+\delta^2_{\varphi^{(\ell,h)},i}+\delta^2_{\psi^{(\ell,h)},i}\right)$	$\frac{1}{6L}\sum_{\ell=1}^{L}\left[\mathrm{CRB}(\alpha^{(\ell,e)})+\mathrm{CRB}(\varphi^{(\ell,e)})+\mathrm{CRB}(\psi^{(\ell,e)})+\mathrm{CRB}(\alpha^{(\ell,h)})+\mathrm{CRB}(\varphi^{(\ell,h)})+\mathrm{CRB}(\psi^{(\ell,h)})\right]$
Dislocation	$\frac{1}{3(L-1)\lambda^2_{\min}}\sum_{i=1}^{I}\sum_{\ell=2}^{L}\left(\delta^2_{\Delta_x^{(\ell)},i}+\delta^2_{\Delta_y^{(\ell)},i}+\delta^2_{\Delta_z^{(\ell)},i}\right)$	$\frac{1}{3(L-1)\lambda^2_{\min}}\sum_{\ell=2}^{L}\left[\mathrm{CRB}(\Delta_x^{(\ell)})+\mathrm{CRB}(\Delta_y^{(\ell)})+\mathrm{CRB}(\Delta_z^{(\ell)})\right]$

Allowing the MLE of prior knowledge that the additive noise has a Gaussian distribution (though this prior knowledge is not needed by the proposed method), the MLE would minimize the objective function,

$$F(\boldsymbol{\mu})=\left\|\tilde{\mathbf{z}}-\sum_{k=1}^{K}\mathbf{a}_k(\boldsymbol{\mu})\otimes\mathbf{s}_k\right\|^2 \tag{45}$$

where the $4LN\times 1$ vector $\tilde{\mathbf{z}}$ is resized from the $4L\times N$ data matrix $\tilde{\mathbf{Z}}$, and $\boldsymbol{\mu}=\left\{\theta_k,\phi_k,\gamma_k,\eta_k,\forall k=1,\ldots,K\right\}$ contains all $4K+12L-7$ number of to be estimated parameters.

The MLE thus equals

$$\hat{\boldsymbol{\mu}}=\arg\min_{\boldsymbol{\mu}}F(\boldsymbol{\mu}), \tag{46}$$

with $F(\boldsymbol{\mu})$ here iteratively evaluated via MATLAB's built-in minimization function "fminunc," which uses the Broyden-Fletcher-Goldfarb-Shanno method, with the stopping criteria of MaxFunEvals $=10^4$ for the maximum number of function evaluations, and MaxIter $=10^4$ for the maximum number of iterations. These iterations are initialized at the ideal electromagnetic vector sensors' nominal values of $g_e^{(\ell)}=g_h^{(\ell)}=1$, $\alpha^{(\ell,e)}=\varphi^{(\ell,e)}=\psi^{(\ell,e)}=\alpha^{(\ell,h)}=\varphi^{(\ell,h)}=\psi^{(\ell,h)}=\Delta_x^{(\ell)}=\Delta_y^{(\ell)}=\Delta_z^{(\ell)}=\epsilon_\varsigma^{(\ell)}=0,\forall\ell$, and the direction-of-arrival initial values are indicated on the figures.

Figure 3 plots the various composite MSE's versus the computational complexity, for the proposed scheme and for maximum likelihood estimation. This computational complexity is measured in terms of elapsed CPU time, as indicated by MATLAB's built-in functions "TIC" and "TOC." The proposed scheme's CPU time consists of time in estimating the array's steering vectors by the "Uni-Vector-Hydrophone" ESPRIT in section 4, for gain uncertainty calibration in solving (12) and (13), for azimuth-elevation directions-of-arrival estimation and polarization estimation in solving (16)–(19) and (22)–(25), for misorientation calibration in solving (34)–(36), for mislocation calibration in solving (40)–(43), and for phase uncertainty calibration in solving (39) and (38). The MLE's CPU time is the time to minimize the objective function in (46) via MATLAB's built-in function "FMINUNC." In Figure 3, the TolFun value for MLE varies from $[10^{-1},10^{-1.5},\ldots,10^{-5.5},10^{-6}]$. The simulation scenario and setting are same as for Figure 2, except that SNR $=25$ dB here.

Figure 3 shows that the MLE would require a computational time *over* 3 *orders-of-magnitude* over that of the proposed method (i.e., the lone circle icon at the lower left corner of each subfigure), for comparable composite MSE's. The MLE has a computational load that increases with the number N of snapshots, but the proposed method's computational load (after forming the data-correlation matrix) is *in*dependent of N. Why is the proposed scheme so much faster in computation? This is because the proposed algorithm (unlike the MLE) needs no exhaustive/iterative search over a high-dimensional parameter space but solves mostly linear equations of low dimensions.

The proposed method is superior over MLE on another consideration: The MLE is predicated on perfect prior knowledge of the noise's full space-time statistics—a demanding and perhaps unrealistic requirement, but not imposed by the proposed scheme.

11. Conclusion

Herein advanced is the first algorithm in the open literature (to the best of the authors' knowledge) to "blindly" calibrate the *intra*electromagnetic vector sensor gain uncertainty, phase uncertainty, and misorientation—as well as *inter*-electromagnetic-vector-sensor dislocation and misorientation. This calibration represents a $(12L+4K-7)$ variate parameter estimation problem, which is broken down here in the proposed method into the five noniterative steps of sections 5 to 9, thereby achieving orders-of-magnitude simplification in computational efficiency over maximum likelihood estimation of the original $(12L + 4K - 7)$ variate problem. These steps and their sequencing exploit quintessential properties of the electromagnetic vector sensor' unique array manifold.

An acoustic counterpart exists [*Song et al.*, 2014] for this proposed electromagnetic acoustic vector sensor calibration scheme. Both the electromagnetic and the acoustic schemes have parallel objectives and motif, but their array manifolds are mathematically distinct, resulting in different high-order sets of parameters to be estimated and different ways to decompose these two high-order parameter estimation problems.

Appendix A: A Counterexample to Disprove Any General Transformation Matrix to Interrelate the Electric Field (or Magnetic Field) Before/After Misorientation

This appendix shows (by a counterexample) that no general transformation matrix (independent of the sources' directions-of-arrival) exists to interrelate *any arbitrary* source's electric field or magnetic field, before and after *any* misorientation. Please refer to section 1.2.

Consider this counterexample: Suppose that there exists a 3×3 matrix $\mathbf{R}^{(\ell)}$ (that is independent of the incident source's direction-of-arrival and polarization) to interrelate the incident source's electric field vector before and after the misorientation in the ℓth electromagnetic vector sensor. This would imply that

$$\mathbf{R}^{(\ell)} = \left[\mathbf{e}_1^{(\ell,e)},\ \mathbf{e}_2^{(\ell,e)},\ \mathbf{e}_3^{(\ell,e)}\right]\left[\mathbf{e}\left(\theta_1,\phi_1,\gamma_1,\eta_1\right),\ \mathbf{e}\left(\theta_2,\phi_2,\gamma_2,\eta_2\right),\ \mathbf{e}\left(\theta_3,\phi_3,\gamma_3,\eta_3\right)\right]^{-1}.$$

The following will give an example where $\mathbf{R}^{(\ell)}$ depends on $\{\theta_k, \phi_k,\ k = 1,2,3\}$. Consider three incident sources at $\theta_1 = \frac{\pi}{3}, \phi_1 = \frac{\pi}{6}, \gamma_1 = \frac{\pi}{4}, \eta_1 = \frac{\pi}{6}, \theta_2 = \frac{\pi}{4}, \phi_2 = \frac{\pi}{3}, \gamma_2 = \frac{\pi}{4}, \eta_2 = \frac{\pi}{4}, \theta_3 = \frac{\pi}{5}, \phi_3 = \frac{\pi}{4}, \gamma_3 = \frac{\pi}{3}, \eta_3 = \frac{\pi}{3}$. Consider a misorientation at $\alpha^{(\ell,e)} = 8°, \beta^{(\ell,e)} = 5°, \gamma^{(\ell,e)} = 3°$ in (6). The above would imply

$$\mathbf{R}^{(\ell)} = \begin{bmatrix} 0.914 + 0.074j & 0.816 + 0.182j & 1.100 - 0.195j \\ -0.076 - 0.006i & 0.791 - 0.208j & -0.264 - 0.142j \\ -0.088 - 0.086j & -0.650 + 0.093j & 0.402 + 0.407j \end{bmatrix},$$

where $j = \sqrt{-1}$. Now change only the first source's direction-of-arrival to $\theta_1 = \frac{\pi}{6}$ and $\phi_1 = \frac{\pi}{3}$. This slight change would now give a very different

$$\mathbf{R}^{(\ell)} = \begin{bmatrix} 0.925 + 0.003j & 0.187 - 0.023j & 0.197 - 0.125j \\ -0.091 + 0.021j & 1.008 - 0.026j & 0.107 - 0.025j \\ -0.069 - 0.032j & -0.129 - 0.009j & 1.009 + 0.005j \end{bmatrix}.$$

Hence, the rotation matrix $\mathbf{R}^{(\ell)}$ depends on sources' directions-of-arrival. Similar counterexamples can be readily constructed to show a similar conclusion with respect to the magnetic field vector.

Hence, despite the orthogonality between $\mathbf{e}(\theta_k, \phi_k, \gamma_k, \eta_k)$ and $\mathbf{h}(\theta_k, \phi_k, \gamma_k, \eta_k)$ in (1) for all $(\theta_k, \phi_k, \gamma_k, \eta_k)$ in the incident electromagnetic wavefield, it is generally false that measurement $\mathbf{e}_k^{(\ell)}$ is orthogonal to the measurement $\mathbf{h}_k^{(\ell)}$ at the ℓth internally misoriented electromagnetic vector sensor. This means that any relative misorientation between the ℓth dipole triad and the ℓth loop triad cannot be calibrated by the angle between the vectors $\mathbf{e}_k^{(\ell)}$ and $\mathbf{h}_k^{(\ell)}$, as mistakenly claimed in equation (2) of *Jia-cai et al.* [2009a], in equation (4) of *Jia-cai et al.* [2009b], and in equations (7) and (8) of *You et al.* [2010]. Likewise, the unnumbered equation below equation (4) in *Wong et al.* [2004] is also incorrect.

Acknowledgments
This work was supported by Hong Kong Research Grants Council's grant number PolyU-152003/15E. The authors would like to thank Petr Tichavský for very useful technical discussions. The authors would like to thank Hasan Saeed Mir for the three points regarding the minimum required number of sources in the last paragraph of section 2. This paper's numerical results are reproducible, based on the equations developed herein and based on simulation settings specified herein.

References

An-jing, Z., Z. Yang, X. Jian, and H. He (2010), An array self-calibration method and DOA estimation for electromagnetic vector-sensor array [in Chinese], *Commun. Technol.*, *43*(4), 161–164.

Appadwedula, S., and C. M. Keller (2006), Direction-finding results for a vector sensor antenna on a small UAV, in *Proceedings of IEEE Workshop on Sensor Array and Multichannel Processing*, pp. 74–78, IEEE, Waltham, Mass.

Au-Yeung, C. K., and K. T. Wong (2009), CRB: Sinusoid-sources' estimation using collocated dipoles/loops, *IEEE Trans. Aerosp. Electron. Syst.*, *45*(1), 94–109.

Belouchrani, A., K. Abed-Meraim, J.-F. Cardoso, and E. Moulines (1997), A blind source separation technique using second-order statistics, *IEEE Trans. Signal Process.*, *45*(2), 434–444.

He, J., and Z. Liu (2009), Computationally efficient 2D direction finding and polarization estimation with arbitrarily spaced electromagnetic vector sensors at unknown locations using the propagator method, *Digital Signal Process.*, *19*, 491–503.

Jia-cai, H., T. Jian-wu, and W. Xiu-lan (2009a), Calibration algorithm against orientation errors of electromagnetic vector sensors [in Chinese], *Acta Electron. Sin.*, *37*(2), 351–356.

Jia-cai, H., T. Jian-wu, and W. Xiu-lan (2009b), Blind DOA and polarization estimation against orientation errors of vector sensor [in Chinese], *Chin. J. Radio Sci.*, *24*(1), 179–184.

Lan-mei, W., L. Gui-Sheng, and W. Hong-yang (2005), Calibration and remedy for vector-sensor [in Chinese], *Chin. J. Radio Sci.*, *20*(5), 687–690.

Lan-mei, W., L. Gui-Sheng, and H. Ji-ying (2007), New calibration and remedy method for gain and phase uncertainty of vector-sensor [in Chinese], *J. Syst. Simul.*, *19*(6), 1326–1328.

Mir, H. S., and J. D. Sahr (2007), Passive direction finding using airborne vector sensors in the presence of manifold perturbations, *IEEE Trans. Signal Process.*, *55*(1), 156–164.

Nehorai, A., and E. Paldi (1994), Vector-sensor array processing for electromagnetic source localization, *IEEE Trans. Signal Process.*, *42*(2), 376–398.

Song, Y., K. T. Wong, and F. Chen (2014), "Quasi-blind" calibration of an array of acoustic vector-sensors that are subject to gain errors / mis-location / mis-orientation, *IEEE Trans. Signal Process.*, *62*(9), 2330–2344.

Wong, K. T. (2001), Direction finding / polarization estimation—Dipole and/or loop triad(s), *IEEE Trans. Aerosp. Electron. Syst.*, *37*(2), 679–684.

Wong, K. T., and X. Yuan (2011), "Vector cross-product direction-finding" with an electromagnetic vector-sensor of six orthogonally oriented but spatially non-collocating dipoles / loops, *IEEE Trans. Signal Process.*, *59*(1), 160–171.

Wong, K. T., and M. D. Zoltowski (1997), Uni-vector-sensor ESPRIT for multi-source azimuth-elevation angle estimation, *IEEE Trans. Antennas Propag.*, *45*(10), 1467–1474.

Wong, K. T., and M. D. Zoltowski (2000), Closed-form direction-finding with arbitrarily spaced electromagnetic vector-sensors at unknown locations, *IEEE Trans. Antennas Propag.*, *48*(5), 671–681.

Wong, K. T., L. Li, and M. D. Zoltowski (2004), Root-MUSIC-based direction-finding and polarization-estimation using diversely-polarized possibly-collocated antennas, *IEEE Antennas Wirel. Propag. Lett.*, *3*(8), 129–132.

You, N., L. Wang, T. Wei, and Y.-Z. Yin (2010), Taylor series approximation for estimation of vector sensor array misorientation, in *International Symposium on Antennas Propagation and EM Theory*, pp. 1224–1226, IEEE, Guangzhou, China.

Yuan, X., K. T. Wong, Z. Xu, and K. Agrawal (2012), Various triad compositions of collocated dipoles/loops, for direction finding and polarization estimation, *IEEE Sens. J.*, *12*(6), 1763–1771.